OPTOFLUIDIC DEVICES FOR BIOLOGICAL AND ENERGY APPLICATIONS

A Thesis

Presented to the Faculty of the Graduate School

of Cornell University

In Partial Fulfillment of the Requirements for the Degree of

Doctor of Philosophy

by

Aadhar Jain

January 2015

© 2015 Aadhar Jain

OPTOFLUIDIC DEVICES FOR BIOLOGICAL AND ENERGY APPLICATIONS

Aadhar Jain, Ph.D.

Cornell University, 2015

ABSTRACT

Optical energy is one of the most ubiquitous form of energy available and as such, has been the source of abundant research into understanding and developing applications using it. The versatility and sensitivity of optical forces have allowed it to be widely applied in both micro/nano scales and macro scales. Herein, I discuss the development of two further devices to take advantage of the numerous benefits offered by optics.

First, a soft gel based optical waveguide is fabricated and experimentally tested. The gel waveguide, fabricated from agarose hydrogel, extends the capability of optical manipulation from silicon and other hard substances to soft materials capable of incorporating biology within the substrate itself. We demonstrate this by incorporating live cells within the core of the optical waveguide where they can be probed by the strong optical field. A microfluidic channel is also integrated thus developing a complete optofluidic configuration for biological studies.

In the second part of this work, the development of a stacked waveguide photobioreactor for algae-based biofuel production is described. The benefits of the thin light paths and uniform light distribution achieved due to the stacked waveguide architecture are demonstrated by investigating biomass growth and ethylene production from genetically engineered

cyanobacteria. Growth rates are found to be eightfold greater than a control reactor, sustained ethylene production is achieved for 45 days, and ethylene production rates two times greater than that of a conventionally run photobioreactor are demonstrated. These capabilities are further improved by optimizing the wavelength and the intensity of the incident light. The thin light paths present in the photobioreactor allow for large carrying capacities with optical densities of over 20 capable of being sustained in the photobioreactor. Optimization of all these parameters led to a further two fold improvement in ethylene production rates leading to an overall fourfold increase over a conventionally run photobioreactor. Besides the experimental verification, theoretical models for light and thermal distribution within the stacked photobioreactors were also created. These results thus provided justification for the stacked waveguide design and exploration for development of a larger scale model.

BIOGRAPHICAL SKETCH

Aadhar Jain graduated with a Bachelors of Technology (B.Tech.) in Mechanical Engineering from Indian Institute of Technology (IIT) Kanpur, Kanpur, India in 2009. He subsequently joined the doctoral program in Sibley School of Mechanical Engineering at Cornell University conducting research under the guidance of Professor David Erickson during the course of his PhD. He was also awarded a Master of Science (M.S.) in Mechanical Engineering in 2013 by Cornell University.

During his term at Cornell University, he served as a research assistant in the Erickson Lab, and as a teaching assistant for two semesters for Fluid Mechanics Laboratory course offered by Professor Charles Williamson. He has presented his research work at international conferences such as Conference on Lasers and Electro-optics (CLEO) and International Mechanical Engineering Congress and Exposition (IMECE). Besides this he has published work in Optics Letters.

Besides his research, Aadhar has been involved in charity work at Cornell volunteering and serving as the coordinator for Asha for Education, a charity working for education of under privileged children in India. He also takes an active interest in playing and organizing cricket at Cornell, as part of the Cornell Cricket Club.

ACKNOWLEDGMENTS

Journey through the five years of doctoral studies could not have been possible without the constant support and help of numerous people. Foremost, my most gracious thanks to my thesis advisor Professor David Erickson for teaching, mentoring and developing me over the years with his help and suggestions, which I am sure, will serve me well further into my career. I gratefully acknowledge my committee members – Professor Clifford Pollock and Professor Abraham Stroock – for their advice and critical suggestions which were very instrumental in finishing my PhD. Funding support provided for my stay at Cornell and my research, by the multiple funding agencies – National Institute of Health (NIH), Advanced Research Project Agency – Energy (ARPA-E), and teaching assistantship provided by Cornell University – was essential for me to finish my studies. I was extremely fortunate to have access to the instruments and staff at Cornell Nanotechnology Science and Technology Facility (CNF) and Nanobiotechnology Centre (NBTC) here at Cornell without which I would have struggled to finish my research.

I would also like to thank my research colleagues – Nina Voulis, Dr. Michael Kalontarov, Dr. Erica Jung, Dr. Devin Doud - with whom I worked with in close collaboration and responsible for a significant portion of the knowledge that I gained through my PhD. Also, thanks to my group mates through the years – Dr.Michael Mak, Dr. Xavier Serey, Dr. Allen Yang, Dr. Pilgyu Kang, Dr. Matthew Mancuso, Dr. Li Jiang, Dr. Mekala Krishnan, Dr. Bernando Cordovez and Dakota O'Dell, Perry Schein, Abdurrahman Gumus, Syed Saad Ahsan – for providing suggestions and comments throughout, and most invaluable discussions on Star Trek, Star Wars and all things science fiction as and when time permitted.

My parents, who kept a check on me and provided invaluable support to me, even while in India deserve a lot of credit for this, as do my brother and sister-in-law, who kept me sane by being a

source of constant amusement. My friends through my stay at Ithaca have kept me involved outside my research and have thus provided a necessary distraction to my research. Finally, to Cornell Cricket Club for playing and keeping me involved with cricket in a small place like Ithaca.

TABLE OF CONTENTS

CHAPTER 1

INTRODUCTION: CENTRAL AIM AND SUMMARY OF RESEARCH

1.1 Central Aim

Optofluidics is a rapidly developing field in which the combination of precision, sensitivity and versatility of optical fields is further combined with the ability to deliver microscale volumes of fluids for interaction with the optical fields. This has led to wide variety of applications especially for study of biological entities of interest. However, the current devices mostly remain confined to the labs with only a few devices developed from soft materials which can be used for implantable *in-vivo* experimentation. This is increasingly important in view of recently developed technologies like optogenetics where it is necessary to precisely probe specific neural cells. In my work, I propose and demonstrate an important step towards developing such a device.

Optofluidics is also being slowly accepted in the field of energy research due to its ability to deliver light precisely at the needed locations. This is especially important in development of biological photobioreactors where the current practice of bringing biology to the source of light is partially responsible for current unviability of photobioreactors for biofuel production. This dissertation focuses on a possible solution to this issue by developing a optical waveguide based photobioreactor, which utilizes the benefits of cheap and well developed methods of light propagation, to achieve this end.

1.2 Brief Overview

This dissertation describes the development of optofluidic devices for i) biological applications where biological entities can be probed by strong core optical fields and ii) improved algal fuel production through optimum light distribution. Chapter 2 provides a summary of relevant literature in the field and provides groundwork for the work described thereafter. Chapter 3 details the fabrication and experimental results of an agarose gel optical waveguide capable of encapsulating live cells. Chapter 4 explains the stacked waveguide photobioreactor design for algal biofuel production and presents results from experiments for algal growth and ethylene production achieved in the photobioreactor. Chapter 5 investigates multiple operational parameters for the stacked waveguide photobioreactor in order to determine the optimal conditions for maximal production rates. With that end, wavelength and intensity of the incident light, along with optical density of the culture are varied and subsequent ethylene production rates are measured. Photosynthetic efficiencies are also calculated to again determine the most efficient set of parameters for operation. Chapter 6 concludes the presented work with a few suggestions for future directions of research. Appendices 1 and 2 contain analytical models for light distribution and thermal conditions within the stacked waveguide photobioreactor. Appendix 3 serves as supplementary information for chapter 5 and details the results of regression analysis performed therein. Appendix 4 describes an analytical model for UV sterilization in a slab waveguide reactor.

1.3 Summary of Research

Aim 1: Development of soft hydrogel waveguide with live cell encapsulation and integrated microfluidics.

- Agarose hydrogel waveguides were fabricated and successful optical waveguiding was demonstrated.
- Live cells were encapsulated within the core of the waveguide, and shown to interact with the core optical field by fluorescent excitation of a live cell stain.
- Soft gel microfluidics was integrated over the hydrogel waveguide.

Aim 2: Development of stacked waveguide photobioreactor with thin light paths for algal biofuel production.

- Benchtop ten stack photobioreactor, consisting of optical waveguides with scattered surfaces for uniform light distribution, was constructed.
- Algal growth was successfully demonstrated within the stacked photobioreactor and growth rates compared to control photobioreactor.
- Ethylene production from a genetically modified cyanobacteria *Synechocystis* sp. PCC 6803 2x EFE grown inside the stacked photobioreactor was measured, and compared against that in a conventionally run photobioreactor.

Aim 3: Optimization of light wavelength, light intensity and carrying capacity of the stacked waveguide photobioreactor.

- Photosynthetically relevant wavelengths, along with multiple incident light intensities, were tested to determine the optimal wavelength and intensity for maximal ethylene production rates.
- Optical density of the algal culture was optimized to determine the carrying capacity of the stacked photobioreactor. Light intensity was again varied to determine the optimum intensity for maximal ethylene production rates.
- Photosynthetic efficiencies for the various operating conditions were determined.

Aim 4: Development of analytical models for light distribution, temperature rise and degree of disinfection for *in-situ* UV sterilization.

- An analytical model was created to estimate the distribution of light across the photobioreactor volume and predict the optimum value of light intensities as a function of culture growth.
- Thermal model was created to predict temperatures within the photobioreactor due to heat generation through non photochemical quenching processes within the photobioreactor.
- A model was created to predict the degree of disinfection for *in-situ* UV sterilization in a single slab waveguide photobioreactor.

CHAPTER 2

LITERATURE REVIEW AND BACKGROUND

Adapted partially from: Chen, Y.-F., Jiang, L.*, Mancuso, M.*, Oncescu, V.*, Jain, A.*, Erickson, D. “Optofluidic Opportunities in Global Health, Food, Water and Energy”. Published in Nanoscale (2012).

*All authors contributed equally

2.1 Optofluidic applications in biology

Researchers have created a number of optofluidic devices by utilizing waveguiding technology and microfluidics to simultaneously localize optical fields and fluid flows to small volumes. Examples of these devices have been used to create biosensors,(Erickson, Mandal et al. 2008; Barrios 2009; Mandal, Goddard et al. 2009) molecular traps,(Chen, Serey et al. 2012) and devices for transporting micrometer and nanometer sized objects.(Yang, Moore et al. 2009; Yang and Erickson 2010) While many of these devices require a significant amount of nanofabrication and may not yet be ready for use in the developing world, a number of recent works have been aimed at creating cheaper and more suitable technologies, including those based on polymers.

One of the earliest works on polymer devices was completed by the Guo group from the University of Michigan in 2002.(Chao and Guo 2002) Since then, his group has demonstrated that these devices could be fabricated into high Q-factor ring resonators,(Ling, Chen et al. 2011) and have used them for biosensing applications.(Chao, Fung et al. 2006) In addition, other groups have attempted to maximize interactions between the optical and microfluidic components of these polymer devices by creating porous waveguide structures and ring

resonators,(Gopalakrishnan, Sagar et al. 2010; Mancuso, Goddard et al. 2012) or soft gel waveguides(Ding, Blackwell et al. 2008). Other groups have used polymers to create photonic crystal structures made of polymers and used them in biosensing applications.(Choi and Cunningham 2006; Choi and Cunningham 2007; Tan, Ge et al. 2011) In one example, Mathias *et al.* show how polymer photonic crystals can be used to detect tumor necrosis factor-alpha (TBF-α) at concentrations as low as 1.6 pg/mL.(Mathias, Ganesh et al. 2008) These devices capitalize on the advantages of polymer devices, *i.e.* their low-cost materials and fabrication, and provide additional advantages by creating material constructs that increase light-matter interactions not easily made in silicon devices.

Recently, novel optofluidic technologies such as anti-resonant reflecting optical waveguides (ARROWs)(Kuhn, Phillips et al. 2010; Measor, Phillips et al. 2011) and rolled-up optofluidic ring resonators (RU-OFRRs)(Smith, Schulze et al. 2011; Smith, Xi et al. 2012) have shown the capability to confine and analyze samples on an individual cell basis. These new techniques demonstrate the high precision and controllability of optofluidics for bioanalysis and the potential to detect trace amounts of pathogens in samples. A second group of devices exists that seeks to integrate plasmonic technologies with microfluidics. Since surface plasmons excited on the surface of metal films are extremely sensitive to the surrounding environment, many plasmonic-based biosensors have been developed in recent years for label-free biosensing.(Anker, Hall et al. 2008) While a number of devices are already commercially available,(Chinowsky, Quinn et al. 2003) many of them do not meet the cost requirements or simple operability required to be used in resource poor settings. In recent work, a number of groups have improved upon these previous devices, creating systems more applicable to

developing countries. One recent example came from Yanik *et al.* in which plasmonic Fano resonances were used to identify protein monolayers through colorimetric changes visible to the naked eye.(Yanik, Cetin et al. 2011)

Gold nanoparticles have also received much attention in the last decade for their use in sandwich-based antigen and DNA detections that rely on local surface plasmon resonance (SPR) shifts,(Storhoff, Elghanian et al. 1998; Storhoff, Lucas et al. 2004; Wilson 2008) as well as silver-deposition enhanced detection assays that resemble enzyme-linked immunosorbent assays (ELISA). The latter detection schemes have been used to identify both oligonucleotide and protein based targets in enzyme-linked immunosorbent assays based on gold nanoparticles, and silver aggregates can be formed around the gold up to sizes that the naked eye and cameras can detect the ligand's presence.(Taton, Mirkin et al. 2000; Nam, Thaxton et al. 2003) Recently, Chin *et al.* used this signal amplification technique in their point-of-care device made of injection-molded plastic. In addition, Fu *et al.* have applied a signal amplification technique to paper microfluidic systems by using a gold-deposition instead of silver.(Fu, Kauffman et al. 2010) Both of these recent examples demonstrate methods of creating devices that can operate almost autonomously without the need for costly infrastructure.

Conventional culture based methods, while reliable and accurate, require days to produce results of the pathogen detection. Therefore, many microscale biosensors have been developed recently to provide rapid detection of pathogens.(Arora, Sindhu et al. 2011) As discussed previously, optofluidics is naturally suited for detection and analysis in very small volumes, and many techniques for disease diagnostics can be applied to food and drink safety.(Fan and White 2011)

The ARROW device mentioned previously is promising for bacteria detection because of its ability to trap and detect a single *E. coli* bacterium with an optical power level of a few microwatts, which is about four orders of magnitude less than conventional optical force traps.(Kuhn, Phillips et al. 2010) The same groups are working to simplify the technology for low resource settings and recently demonstrated an ARROW design with an integrated on-chip spectral filter for multiple optofluidic detection uses (Fig. 5).(Measor, Phillips et al. 2011) As the authors point out, the filter technology developed could benefit other optical sensing methods that have also been used to detect foodborne bacteria such as Förster resonance energy transfer (FRET)(Olsen, Gibbins et al. 2009) and surface-enhanced Raman scattering (SERS).(Fan, Hu et al. 2011)

Despite development of such multitude of optofluidic devices, there remains a lack of devices that allow the strong optical fields inside an optical waveguide to interact directly with the biological entity of interest. This is since majority of the optofluidic devices are fabricated on hard substrates where such interaction is impossible to create. On the other hand, current methods for fabrication in softer materials like hydrogels are incompatible with biology due to the harshness of the treatment involved during fabrication. However, fabrication of such devices would be valuable, especially in newly emerging fields like optogenetics where the application is fundamentally based upon interaction of cells with strong optical fields for excitation. Therefore, in order to develop highly targeted optogenetic devices for *in-vivo* applications (Choi, Choi et al. 2013), it is necessary to investigate devices capable of live cell encapsulation within the waveguides themselves. This is discussed in further detail in Chapter 3.

2.2 Optofluidic applications for renewable energy

It is estimated that around 1.6 billion people currently lack access to electricity, with a majority of these residing in developing countries,(Ahuja and Tatsutani 2009) which leads to a poor quality of life. Further, the majority of the existing electricity generation in developing countries is through non-renewable sources like coal and oil(Ahuja and Tatsutani 2009) – resources which are becoming increasingly scarce and subsequently expensive. Moreover, additional use of these resources could significantly worsen global warming due to increased carbon emissions. In such a scenario, it is in the interest of these countries to develop renewable energy sources that can be either converted to electricity or used for heating and lighting purposes directly. Solar power, being the most abundant and widely available resource,(Jacobson and Delucchi 2011) is an obvious choice to explore and develop.

Even though solar photovoltaic cell technology has been developed significantly over the years, the costs associated with it are still large,(Ahuja and Tatsutani 2009) with infrastructural and maintenance costs making infeasible for large-scale adoption in developing countries. In such a scenario, it is advisable to develop 'off-grid' resources that can be employed locally and therefore avoid high infrastructural costs.

One of the more attractive alternatives is the development of photocatalytic fuel production – a process in which photo activated catalysts are used to drive chemical reactions for fuel production. One of the more popular examples is the splitting of water molecules to produce oxygen and hydrogen, which can be stored and used as a fuel. This technology has been dubbed as "artificial photosynthesis" due to the similarities with the natural photosynthesis process

exhibited by plants. In a similar vein, Nocera and colleagues have recently reported the development of an 'artificial leaf'(Reece, Hamel et al. 2011) – a silicon cell coated with catalysts, which when placed in water and exposed to sunlight starts producing hydrogen without the need of any external wires or instrumentation. Another group has demonstrated an artificial photosynthesis process on a microfluidic chip making use of the efficient transport characteristics offered by microfluidics to enhance the efficiency of the fuel production process.(Lee, Lee et al. 2011) Recently, Hoang *et al.* demonstrated a photocatalyst that can operate in the visible spectrum, which can lead to a significant improvement in the efficiency of these devices under ambient sunlight.(Hoang, Guo et al. 2011) We refer the readers to a recent review by Erickson *et al*. for a detailed discussion on the state of the art photocatalytic technology and its various optofluidic prospects.(Erickson, Serey et al. 2011)

Photobioreactors, which are devices that use photosynthetic microorganisms such as algae or cyanobacteria for producing higher energy fuels using sunlight and carbon dioxide, represent another important source for production of biofuels. Biomass fuels are important source of household energy in developing countries and especially in many African countries where it is estimated to provide energy to nearly 90 percent of the households.(Kammen 2006) However, currently most of the fuel needs are met by burning wood or charcoal, neither of which is good for the environment, and is in increasing danger of being depleted.(Kammen 2006) Further, these fuels are highly inefficient and produce pollutants that have been linked to a large number of deaths.(Kammen 2006) Other options include using crops such as corn or soybean for the production of biodiesel. However, this would put them in direct competition with food crops for the limited arable land and fresh water sources available for agriculture,(Searchinger, Heimlich

et al. 2008) which are already insufficient for feeding the growing populations in developing countries. Photobioreactors, on the other hand, can be developed in non-arable land and algae and bacteria can be grown using seawater or even wastewater.(Campbell 2008; Larkum, Ross et al. 2012) Further, a number of algae and bacteria have been identified and genetically optimized for the production of fuels.(Larkum, Ross et al. 2012) One of the main technological challenges is the design of photobioreactors so that they can be optimized for both sunlight capture and distribution, and developing efficient fluidics for efficient nutrient and fuel transport leading to maximum production of biomass and fuel per unit area. For example, Ooms *et al*. recently demonstrated use of evanescent light from TIFR for production of fuel from a cyanobacteria.(Ooms, Sieben et al. 2012) .

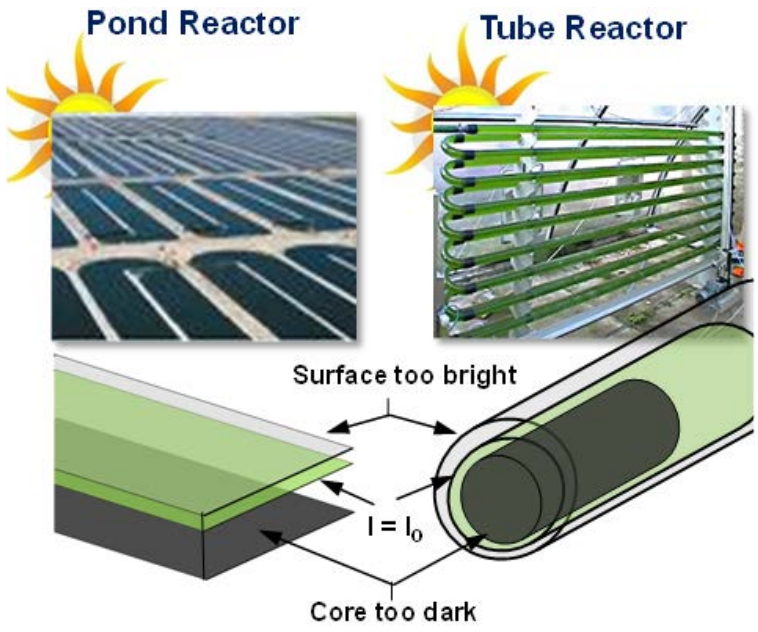

Figure 2.1: Limitation of light distribution in traditional photobioreactors. Exposed surfaces lead to photoinhibition while surfaces too deep are photolimited due to shading by cells above. (Image courtesy : Professor David Sinton)

Current photobioreactors are however limited by non-uniform distribution of light within the reactor volume due to self shading effects of the cells (**Figure 2.1**) (Erickson, Sinton et al. 2011). At present, this is alleviated by various mixing strategies which involve substantial capital and operational costs and energy, which are one of the reasons for lack of commerciably viable algal biofuel production plants. Further, studies have indicated that this leads to energy return on investment of less than one – an unattractive proposition for a renewable energy source. Therefore, it requires an important shift in design principles to solve the problem. Since mechanical mixing strategies required to bring algae to the source of illumination are energy and capital intensive, while delivery of optical energy is cheap and easy, as demonstrated by the widespread use of waveguiding technologies (*for e.g.* optical fibres) around us, it might be more valuable to bring this paradigm to photobioreactors too. This is illustrated in **Figure 2.2** using stacked optical waveguides and discussed in further details in Chapter 4 and 5 of this dissertation.

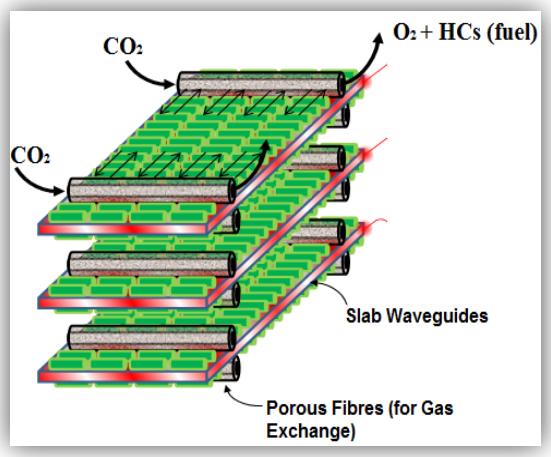

Figure 2.2: Illustration of stacked waveguide photobioreactor concept. Light is delivered to the algae directly by propagating them from the coupling source through optical waveguides. The optical waveguides can then be stacked for development of compact photobioreactors (Image courtesy : Professor David Erickson)

CHAPTER 3

GEL-BASED OPTICAL WAVEGUIDES WITH LIVE CELL ENCAPSULATION AND INTEGRATED MICROFLUIDICS

Adapted from: Aadhar Jain, Allen HJ Yang, and David Erickson. Published in Optics Letters(2012).

3.1 Abstract

In this letter, we demonstrate a biocompatible microscale optical device fabricated from agarose hydrogel that allows for encapsulation of cells inside an optical waveguide. This allows for better interaction between the light in the waveguide and biology, since it can interact with the direct optical mode rather than the evanescent field. We characterize the optical properties of the waveguide and further incorporate a microfluidic channel over the optical structure, thus developing an integrated optofluidic system fabricated entirely from agarose gel.

3.2 Introduction

On chip optical methods for biological applications, varying from biosensing (Dancil et al., 1999; Fan et al., 2008; Homola et al., 1999) to optical trapping and manipulation (Ashkin and Dziedzic, 1987; Yang et al., 2009) are becoming increasingly prevalent. A majority of such optical devices are fabricated out of rigid materials like silicon or silicon nitride, which do not allow for biomolecular access to the energy rich core field of the optical waveguide. A related area that has attracted increased attention of researchers has been in developing optical devices using hydrogels(Ding et al., 2008; Koo et al., 2003; Sowa et al., 2006; Wang et al., 2010) . Hydrogels are attractive since they are biocompatible and can be designed to respond to, or sense, different external stimuli like pH(Park, 1999; Richter et al., 2008), temperature (Park, 1999; Tanaka, 1978) or light (Suzuki and Tanaka, 1990). However, the harsh methods used in fabrication of hydrogel waveguides, for example femtosecond lasers (Ding et al., 2008) or UV irradiation (Koo et al.,

2003), are incompatible with embedding biological material inside the waveguides and are therefore, also dependent on the weak evanescent near field for their operation. Here we demonstrate a hydrogel waveguide, fabricated out of agarose, which allows for incorporation of biomolecules and cells inside the core of the waveguide.

Agarose, a polysaccharide derived from agar, is a popular material for constructing biocompatible gels for the purpose of DNA separation through gel electrophoresis. Agarose hydrogel is known to be structurally strong enough to be molded into microscale structures(Ling et al., 2007; Stevens et al., 2005) while providing the additional ability to encapsulate live cells in the gel (Ling et al., 2007; Moskaluk and Stoler, 2002). On measurement of the refractive index of the agarose hydrogel, we found that it varied appreciably with the concentration of agarose in it. A change of concentration by 0.5% (w/v) yields a change of around 0.001 in refractive index – a large enough change for effectively guiding light in an optical waveguide.

3.3 Materials and Methods

3.3.1 Fabrication of Optical Agarose Gel Waveguides

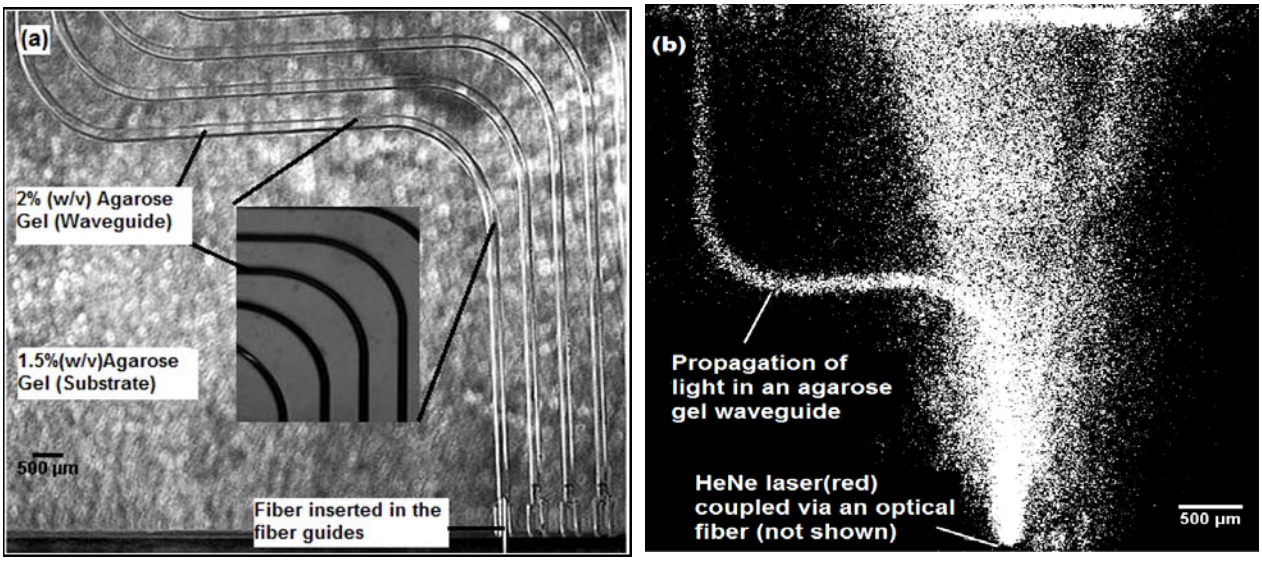

Figure 3.1 Optical agarose gel waveguide (a) Agarose gel waveguide with 2% (w/v) gel as core and 1.5%(w/v) gel as substrate (Inset: Magnified view), (b) Gel waveguides with HeNe laser (630 nm) coupled into the waveguide**.** Light scattered from the gel waveguide is seen.

In our device, both the substrate and core of the optical waveguide were fabricated from hydrogels made from high strength agarose (USB Agarose High Gel Strength). To fabricate the substrate, a gel solution was prepared by adding powdered agarose slowly to a heated solution of distilled water, until the agarose melted and a clear solution containing 1.5% (w/v) agarose was obtained. The solution was then kept in a water bath at 80^0C for 45 minutes to allow any air bubbles to diffuse out of the solution. The solution was finally allowed to cool in petri dishes to obtain a smooth gel surface. Gel optical waveguides were then created through a soft lithography process using poly (dimethylsiloxane) (PDMS) (Ellsworth Adhesives) stamps (Ling et al., 2007; Stevens et al., 2005). A SU-8 master was fabricated on a silicon wafer using standard photolithography techniques and used to mold the PDMS stamps (a negative replica). The PDMS stamp was exposed to oxygen plasma in a vacuum chamber in order to render it hydrophilic and remove formation of any air pockets or bubbles during fabrication (Stevens et al., 2005). A 2% (w/v) agarose solution was similarly prepared and a small amount of solution (~500 µl) was carefully pipetted out and then slowly poured on the substrate. The stamp was then slowly pressed upon the hot agarose solution and left to cool in the air for 20 minutes under a small weight (200g), to allow the solution to gel into the required features. The PDMS stamp was then carefully and easily stripped off from the agarose substrate, yielding the structure as shown in **Figure 3.1(a)**. The waveguides thus fabricated were designed to be multimoded rib waveguides with cross sectional dimensions of 130 µm x 130 µm.

The refractive indices of the two different concentration gels – 1.5% (substrate) and 2% (core) – were separately measured to be 1.3343 and 1.3357 using a digital refractometer (Sper Scientific). In order to test the gel waveguides, coupling experiments were carried out using a 633 nm (red) laser source and was coupled into the waveguides using a multimode fiber (Thor Labs AFS105/125Y). As can be seen from Figure 1a, alignment between the fiber and the gel waveguides was facilitated through the use of 'fiber

guides' designed and fabricated along with the waveguides themselves, removing the need to 'cut' the waveguides. The gel waveguides were found to couple light easily, as shown in **Figure 3.1(b)**.

3.3 Results and Discussion

3.3.1 Scattering and Absorbtion Losses

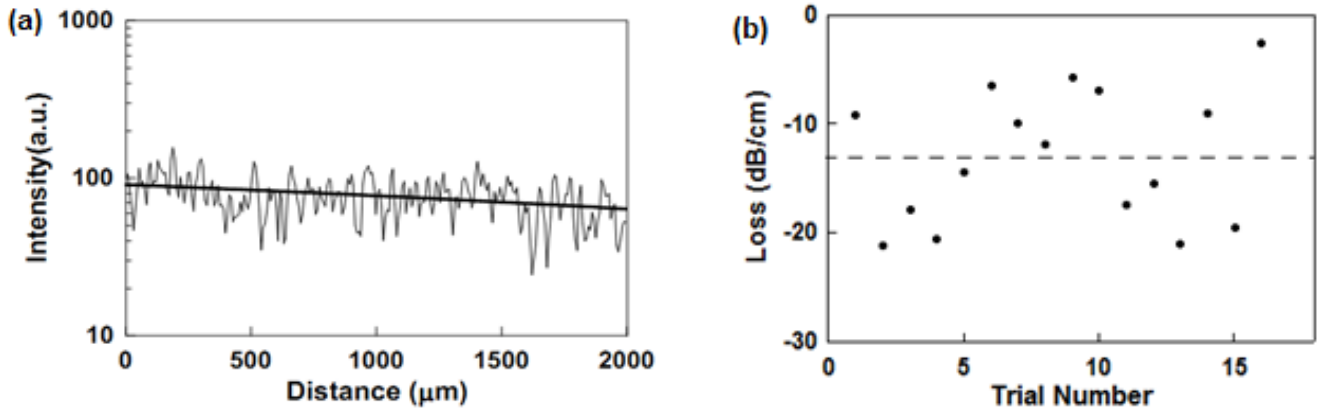

Figure 3.2 Scattering and absorbtion losses in agarose gel waveguides (a) Intensity variation along a typical gel waveguide for estimation of scattering/absorption losses. (b) Scattering/absorption losses measured across different waveguides. Dotted line indicates average measured loss

An important consideration for optical propagation is the scattering/absorption losses suffered by the light propagating in the waveguide. We quantified these losses in our waveguides through image analysis using ImageJ. Briefly, we measured the intensity of the scattered light, as seen from an overhead image, along the length of the waveguide. Care was taken to avoid saturation of pixels and to account for any background illumination. Assuming that the scattered intensity is proportional to the intensity of light propagating in the waveguides, the intensity map so obtained (and shown in **Figure 3.2(a)**) was plotted on a semi log map in order to determine the loss in dB per unit length. **Figure 3.2(b)** shows the measurements done across different waveguides on different chips and the resultant grouping of loss measurements demonstrates the repeatability of the fabrication process. We obtained an average loss of

13 dB/cm. As comparison, reference (Foorster et al., 2009)reported losses of 5-10 dB/cm for alginate hydrogels and 2-7 dB/cm for synthetic hydrogels for 1.1 mm diameter waveguides. Even though higher concentrations of gel could lead to a better index contrast, it would be accompanied with an increase in stiffness of the gel and a decrease in the pore size of the gel. This would move it away from the stiffness found in actual physiological environments, and the smaller pore size would inhibit the motion of biomolecules, nutrients *etc*. through the gel. Additionally, a small refractive index change by increasing the concentration(~0.001) would affect the scattering losses only minimally due to its weak dependence on refractive index (Ding et al., 2008).

3.3.2 Integration of Microfluidic Channels

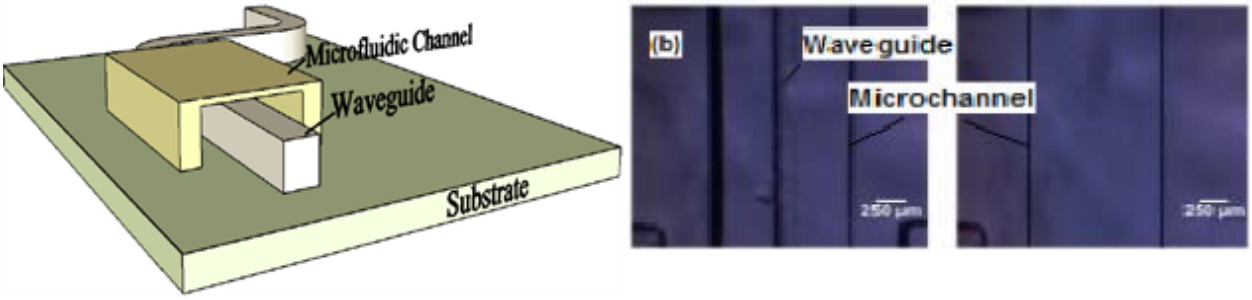

Figure 3.3 Incorporation of microfluidics over optical gel waveguide (a) Schematic of an open end microchannel design (not to scale). Open ends are later sealed by low melt agarose (b) Flow inside the microchannel: After sealing the microchannel, a gel waveguide within the microchannel is imaged before (left) and after (right) flowing blue food color through the microchannel.

For integrated on-chip bio applications, it would be ideal to incorporate a fluidic channel on the optical chip, thus allowing for flow of analytes or media over the optical elements. Though Ling *et al.* (Ling et al., 2007), among others (Cheng et al., 2007), have reported microfluidic channels using agarose hydrogel, their method involved heating the substrate surface (which were featureless) to seal the microchannels. Due to the optical waveguides present on the substrate in our device, we could not apply a

similar methodology. In order to overcome this obstacle, we opted for a novel 'open–end' microfluidic channel design. Briefly, as shown in the schematic in **Figure 3.3(a)**, both the ends of the microchannel were cut open, after which it was aligned, along its length, with the optical waveguide, so that no part of the microfluidic layer came in direct contact with the optical waveguides.. The channels were then sealed, both along the sides and at the open ends, using a low melt agarose solution (USB Agarose – Low Melt) at around 40^0C, which gelled to form a tight sealing. Steel tubing (Small Parts) was used to provide access ports for pumping fluids in through the channel. **Figure 3.3(b)** shows the flow experiments performed using blue food color, and demonstrates the efficacy of the fabricated fluidic channel.

3.3.3 Encapsulation of Live Cells within the Agarose Waveguides

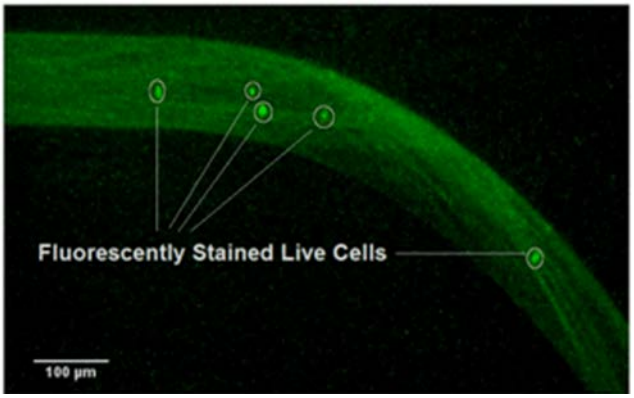

Figure 3.4 Encapsulation of live cells within an optical gel waveguide: Gel waveguide with Calcein stained MDA-MB231 cancer cells embedded within the core of the waveguide and coupled to an Argon laser (488 nm). The waveguide has been imaged under a fluorescent microscope and live cells have been encircled for clarity.

In order to demonstrate the bio compatibility of our fabrication process, we embedded live cells in the agarose waveguides. We used the metastatic breast cancer cell line – MDA-MB231 – for our experiments. The cells were subcultured in cell media DMEM (Invitrogen #11965-092) supplemented with 10% horse serum, were fed every second day and passaged every 3 days at a subculture ratio of 2:5.

The substrate (1.5% w/v agarose gel) and plasma treated PDMS stamps were fabricated as described earlier. A 4% (w/v) agarose solution was prepared in a similar fashion, and maintained at 70^0C in a water bath for 60 minutes to dissipate any air bubbles. A suspension of cells in the subculture media was then mixed with an equal volume of the prepared agarose solution to yield a 2% agarose solution with suspended cells. The fabrication of the waveguides was carried out using the PDMS stamps, as detailed before. The above steps were carried inside a biosafety hood to maintain sterile conditions. The optical waveguides, now embedded with cells, were left under cell media at 37^0C in a 95% air / 5% CO_2 incubator for 24 hours. Cell viability was then assessed by Calcein AM live cell stain. After incubating the waveguides for 30 minutes further, a 488 nm Argon laser was coupled into the waveguides to excite the Calcein stain and was observed under a florescence microscope. As can be seen from **Figure 3.4**, the subsequent image confirms the cells, which are now embedded inside the waveguides, to be alive. We note that the background signal seen from the agarose is due to the scattering of the propagating light. Preliminary measurements indicated that the propagation losses for the cell embedded waveguides were of the same order as before (~12-13 dB/cm). Cell viability was separately confirmed by observing an embedded cell, after incubation within the gel waveguide for 24 hours, over a period of 12 hours. Supplementary Video 1 shows the cell in constant movement over the observation period. We believe that the movement is caused by the extension of multiple pseudopodia by the cell in an attempt to attach to the gel matrix. But the absence of adhesive proteins in agarose prevents the cell from actually adhering to the matrix. However, this could be alleviated by adding chitosan (Cao et al., 2009) or gelatin (Sakai et al., 2007) to the agarose solution

3.4 Conclusion

In conclusion, we have demonstrated a gel optical platform capable of live cell encapsulation within the core of the optical structures. We have further incorporated microfluidic channel over the waveguides to allow for integrated opto-fluidic operation. We believe that this platform can be extended to perform force experiments on cells, akin to those performed typically by optical tweezers, in a 3D extracellular matrix (ECM) like environment offered by agarose gel. Additionally, these can also be used for simultaneously sensing any changes to the cell as physical and chemical cues are provided to it. We also found the process to be compatible with DNA encapsulation (results not shown), and we believe it should further allow for a wide variety of biological entities, like proteins, to be incorporated inside optical waveguides.

CHAPTER 4

STACKED OPTICAL WAVEGUIDE PHOTOBIOREACTOR FOR HIGH DENSITY ALGAL CULTURES

Adapted from: Erica E. Jung[‡], Aadhar Jain[‡], Nina Voulis, Devin D. R. Doud, Largus T. Angenent, and David Erickson. Submitted to Bioresource Technology.

‡Both authors contributed equally to the work.

4.1 Abstract

In this work, an ultracompact algal photobioreactor that alleviates the problem of non- optimal light distribution in current algae photobioreactor systems, by incorporating stacked layers of slab waveguides with embedded light scatterers, is presented. Poor light distribution in traditional photobioreactor systems, due to self-shading effects, is responsible for relatively low volumetric productivity. The optimal conditions for operating a 10-layer bioreactor are outlined. The bioreactor exhibits the ability to sustain uniform biomass growth throughout the bioreactor for three weeks, and demonstrates an 8-fold increase in biomass productivity. Using a genetically engineered algal strain, constant secreted ethylene production for over 45 days is also demonstrated. Since the stacked architecture leads to improved light distribution throughout the volume of the bioreactor, it reduces the need for culture mixing for optimum light distribution, and thereby potentially reducing operational costs.

4.2 Introduction

Biofuels derived from algae represent a promising source of alternative fuel that could help meet ever increasing energy demands and address rising concerns with regards to carbon emissions leading to global warming (Chisti, 2007; Mata et al., 2010). Microalgal systems – consisting of single cell photoautotrophic eukaryotes or cyanobacteria – are an attractive feedstock for biofuel due to their independence from soil fertility (*i.e.* they do not compete with arable land area or

forest ecosystems for their development) (Chisti, 2008; Stephens et al., 2010), relative independence from seasonal cycles allowing for year round production, high oil content (as percentage of biomass) (Chisti, 2007), and significantly higher productivity rates as compared to oilseed crops (Brennan & Owende, 2010; Chisti, 2008). Further, their water requirements, despite being grown in aqueous media, are often less than those for terrestrial crops, and can, in principle, be satisfied with even brackish water, reducing the ever increasing demand on freshwater sources (Brennan & Owende, 2010).

Currently, the most popular systems for commercial production of algal biomass for biofuels are so-called open systems – including natural, circular, or raceway ponds (Chen et al., 2011; Rodolfi et al., 2009; Zittelli et al., 2013). Raceway ponds consist of interconnected circuits of fluid channels with the microalgae suspension being continuously mixed by paddle wheels (Zittelli et al., 2013). The relatively low capital cost associated with these bioreactors adds to their popularity, but they do suffer from a number of operational and control problems related to evaporation, temperature fluctuations, sensitivity to culture contamination, and other environmental factors such as rainfall (Zittelli et al., 2013). These issues have led to development of closed photobioreactor systems, which provide a more controlled environment, and thus increased protection from external contamination and improved control over culture and media conditions. A number of closed photobioreactors have been developed including flat, tubular, manifold, and biofilm bioreactors (Chen et al., 2011; Lehr & Posten, 2009; Zittelli et al., 2013). Generally speaking the increased capital costs of these reactors are offset by the operational advantages outlined above (Chisti & Yan, 2011).

In all these bioreactors, adequate light supply and distribution across the bulk of the algal culture is a key factor affecting productivity (Chisti, 2007). An overabundance of light, typically at the

illuminated surface, can lead to photoinhibition (Brennan & Owende, 2010; Janssen et al., 2003; Rubio et al., 2003), while insufficient penetration of light into the culture (*e.g.* due to self-shading effects) leads to optically dark regions incapable of supporting optimal growth. To avoid outer regions with excessive illumination and inner regions with insufficient light, photobioreactors require high surface to volume ratios allowing light to be distributed to as large a fraction of the culture as possible. Most photobioreactor designers attempt to resolve the illumination problem by actively mixing the culture volume to expose the algae, on an average, to sufficient number of photons (Janssen et al., 2000; Molina Grima et al., 1999). However, these active mixing mechanisms tend to be energetically demanding and lead to higher operational costs (Chisti, 2007; Molina Grima et al., 1999). This is one of the reasons that the energy return on investment (EROI) – ratio of energy produced to energy input to the system - for algal biosystems is relatively low compared to other fuel sources, and in some cases has been estimated to be less than one (Beal et al., 2012b). Development of photobioreactors that can provide optimal light delivery with a reduced requirement for active mixing would, therefore, be of significant interest (Chisti & Yan, 2011).

To mitigate the effect of poor light distribution, photobioreactors with internal light distribution and guiding structures have been developed. Techniques that have been demonstrated include the use of: surface plasmon based light back scattering (Torkamani et al., 2010), LED array panels (Choi et al., 2013; Lee & Palsson, 1994), optical fibers (An & Kim, 2000; Chen et al., 2006; Xue et al., 2013), and planar waveguides (Dye et al., 2011; Janssen et al., 2003). Most of the studies were applied to relatively low density algae cultures (~OD 3), whereas high production systems necessitate high-density cultures. (Ooms et al., 2012) and (Jung et al., 2012) recently demonstrated single layer slab-waveguide systems that used near surface evanescent

fields for algal growth and characterized the spatial-temporal growth patterns. The “stackable” nature of these single-layer systems is attractive in that it allows for increased productivity on a limited land area. However, the shallow depth of the evanescent field near the waveguide surface limits overall achievable biomass accumulation, thereby requiring a large number of stacks, which significantly increases capital costs.

Leveraging the advantages of short-light path design and eliminating the limitations of evanescent field illumination, a 10-stack photobioreactor with integrated slab waveguides that incorporate scattering surfaces was developed, enabling light to escape the waveguide surface and penetrate deep inside the bioreactor, resulting in uniform algae growth with considerably higher volumetric production rates. The performance of the bioreactor is quantified in two ways: biomass accumulation with time and volumetric ethylene production rates from a genetically engineered strain (Ungerer et al., 2012). Uniformity of biomass accumulation is evaluated by measurement of surface coverage of the bacterial colonies on the waveguide surface, and change in optical density (OD_{730}) across the stacks. The change in OD_{730} is compared to a control without internal waveguides to gauge the benefits of even distribution of light facilitated by the use of internal waveguides. In the second section, the capability of the stacked photobioreactor to sustain consistent production rates is evaluated by measuring ethylene production rates from an engineered strain for 45 days. Finally, a conventional flat plate photobioreactor with a 3-cm light path was assembled and run to provide a baseline ethylene production rate to compare against the production rates achieved in the stacked photobioreactor

4.3 Materials and Methods

4.3.1 Fabrication and Assembly of the 10-stack photobioreactor

A 3D printer (Connex 500, Objet Geometries Inc, Rehovot, Israel) was used to print a frame of the 10 stack photobioreactor. A photocurable resin (VeroClear, Objet Geometries Inc, Rehovot, Israel) was used for the 3D printing. The printed frame was then coated by parylene C to prevent gas and liquid leakage. The photomask was also printed using the same photocurable resin and was subsequently covered by aluminum foil to reflect light that was not coupled into the slab waveguides. After waveguides were assembled into the frame, residual gaps between waveguides and the frame were sealed by flowing PDMS in the gaps and subsequently curing it. The dimensions of the fabricated bioreactor were 2.5cm in width, 3cm in height, and 7.5 cm in length with a 2-mm light path between two waveguides.

4.3.2. Fabricating waveguide samples

Optical waveguides were fabricated using standard borosilicate glass slides (VWR VistaVisio Microscope Slides, Radnor, Pennsylvania) and cover slips (VWR Micro Cover Glasses). The borosilicate glass slides were chemically etched to create a scattering surface for allowing the light within the waveguide to escape out. A glass etching cream (Armour Etch, Hawthorne, New Jersey) was applied to the glass slide for seven hours, after which the glass slide was soaked in water to remove the residual etching cream. Light scattering from the surface was further improved by incorporating air cladding (instead of liquid cladding) by affixing cover slips to provide an air cushion. This creates a higher contrast in refractive indices between the waveguide and the cladding to maximize the intensity of scattered light from the surface of the waveguide. Uncured Polydimethysiloxane (PDMS) (Dow Chemicals, Midland, Michigan) was used as a

resin to permanently fix coverslips on the etched glass slide by curing PDMS at 80°C for two hours

4.3.3 Growth of the inoculum culture

A genetically modified strain (termed *Synechocystis* sp. PCC 6803 2xEFE) (Ungerer et al., 2012) of cyanobacteria *Synechocystis* sp. PCC 6803, which are often also called blue-green algae (Corbett & Parker, 1976; Sharma et al., 2011; Steffensen et al., 1999), was used for experiments and served as a model organism for continuous biofuel production. Semibatch cultures providing the initial inoculum for the stacked photobioreactors were grown in gastight 1 L Schott bottles with 20 ml of the *Synechocystis* sp. PCC 6803 culture grown under a headspace containing a 5% CO_2 atmosphere. The culture media consisted of standard BG-11 medium, augmented with 20 mM $NaHCO_3$ as an additional carbon source, and 4.6 g/L TES as buffering agent. All cultures were grown in media with 25 mg/L spectinomycin and 200 mg/L kanamycin (Ungerer et al., 2012). Antibiotics are added to prevent the ethylene producing strain, which has been genetically modified to be resistant to the antibiotics, from reverting back to the wild-type strain or being outcompeted by the latter. The culture was grown at 30°C and 100 µE m^{-2} s^{-1} broad-spectrum light. The semibatch culture was maintained at OD_{730} of 60. Inoculum for 10-stack bioreactors was diluted to the required starting OD_{730}.

4.3.4 Image analysis

The surface coverage of bacterial colonies, *i.e.* the ratio of the suface of the waveguide covered by bacterial colonies to the entire surface area of the waveguide, was measured by obtaning fluorescent images of *Synechocystis* sp. PCC 6803 2x EFE. The measurement provided an estimate of the spatial uniformity of biomass accumulation, which in turn is indicative of

distribution of light within the stacked waveguide photobioreactor. The cyanobacteria were cultured on the waveguide for 21 days and quantitatively analyzed by the method published previously (Kalontarov et al., 2013).

The surface coverage of bacterial colonies on the waveguide was calculated by first subdividing the obtained fluorescence images in 128-by-128 pixel squares. In each square the number of pixels which contained algae was identified (*i.e.* pixels that have higher grey values than a threshold value of fluorescent signals from bacteria), which was then divided by the total number of pixels in the square. This calculation yielded the local surface density expressed as a percentage.

4.3.5 Gas Extraction and Analysis

After each experimental run, the gaseous products were collected through the septum at the output port using syringes, while the influent port was connected to a bottle containing displaced algal culture. As the gas was pulled out from the reactor using the syringe, the liquid culture displaced earlier was pulled back into the bioreactor, ensuring that there was no dilution of the gas samples in the reactor by ambient air. The entire volume of the gaseous products was thus collected. Gas samples were analyzed using a gas chromatograph (GC) optimized for ethylene measurements; the GC was equipped with an alumina-silica column (181°C, He carrier gas at 20 mL/min), and a flame ionization detector (FID) with hydrogen fuel gas (25 mL/min H2 at 204°C). Thus, by knowing the concentration of ethylene in the gas samples, the volume of the collected gas and the duration of the run, the corresponding production rate for ethylene could be determined.

4.3.6 Conventional Flat Plate Photobioreactor

A 4.5-L flat-plate photobioreactor was run semi-continuously and used as a benchmark for the ultra-compact bioreactors. During the operating period, the photobioreactor was continuously aerated with ambient air at a gas flow rate of 1.5 L h^{-1} to provide the culture with CO_2 and to ensure sufficient mixing of the culture. The photobioreactor was subjected to light-dark cycles (0.5 h dark followed by 0.5 h light) at 200 µE m^{-2} s^{-1}, illuminated from one side with a light path of 3 cm. The main dissolved minerals (Cl^-, SO_4^{2-}, PO_4^{2-} and NO_3^-) were monitored 3 to 5 times a week and the photobioreactor was fed semi-continuously when mineral nutrient composition was found insufficient. The photobioreactor pH was monitored daily and adjusted manually to pH 8.5 ± 0.25 using 1M HNO_3.

4.4 Results and Discussion

4.4.1 Surface modifications for light scattering

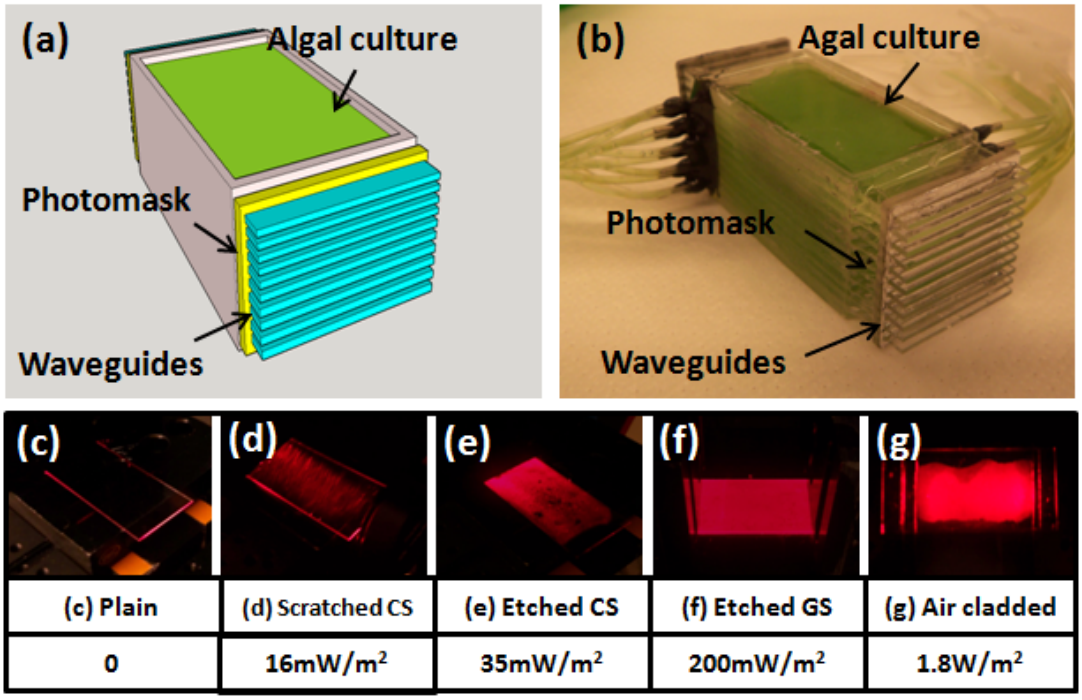

FIGURE 4.1 Design of the Ten–Stack Photobioreactor: (a) A schematic of the ten stack waveguide photobioreactor. **(b)** Prototype ten stack waveguide photo bioreactor. **(c) - (g)** Modified surfaces to enhance light scattering; (c) plain coverslip, (d) mechanically modified coverslip (CS), (e) chemically etched coverslip (CS), (f) chemically etched glass slide (GS), (g) chemically etched glass slide with an air cladding. Values in the table represent light intensities measured on top of modified surfaces.

The bioreactor consisted of the 3D printed frame to hold 10 slab waveguides for delivering light to microalgae, and the photomask to block uncoupled lights (i.e. light that does not enter the slab waveguides and is, therefore, not propagated through the waveguides) (**Figure 4.1(a) and Figure 4.1(b)**). To optimize light scattering from the surface of an optically excited waveguide, different methods of surface modification were examined. First, a coverslip (light incident area ~3.5 mm^2) was modified mechanically by forming defects on the surface by using sand paper (**Figure 4.1(d)**). When light intensity of 3W m^{-2} was coupled to one end of the coverslip, an

intensity of 16 mW m^{-2} was measured on top of the modified surface. Alternatively, a coverslip was chemically modified by using a glass etching cream (**Figure 4.1(e)**). Light scattering from the chemically etched surface of the coverslip was measured to be twice as high as light scattered from a mechanically modified cover slip shown in Figure 4.1(e). This was further enhanced by utilizing glass slides with a larger light incident area (~25 mm^2) to couple the incident light into. As a result, the light intensity measured on the chemically etched surface of glass slide was 6 times higher than that measured from the chemically etched coverslip (**Figure 4.1(f)**). The surface scattering was maximized by integrating a coverslip on the etched side of the glass slide (**Figure 4.1(g)**). This integration created an air cladding that promoted light scattering by allowing larger difference in refractive indices (1.45 to 1.33 when the glass slide is in contact with water directly vs. 1.45 to 1 when the etched side is cladded by air). Overall, a maximum scattering efficiency of 60% (of the coupled light) was achieved using the air cladded waveguides, which resulted in a 50-fold improvement as compared to the etched coverslips. Based on the significantly higher scattered intensity measured from air cladded waveguides, these were assembled in the experimental bioreactors as described in Methods.

4.4.2 Spatial-temporal uniformity of algae biomass inside the photobioreactor

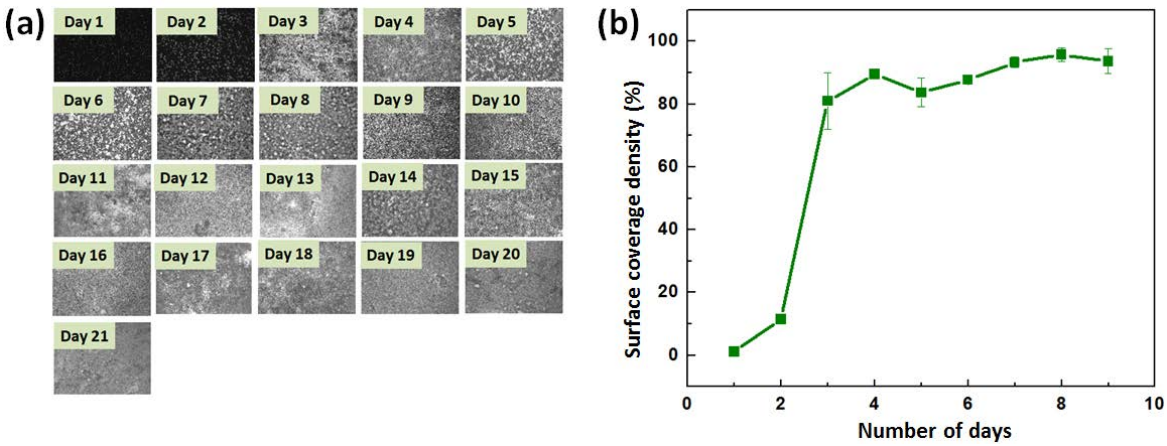

FIGURE 4.2 Algal growth in the Ten-stack Photobioreactor: (a) Time series of biomass accumulation observed on the surface of the waveguide in the ten-stack photobioreactor. Fluorescent signals of the *Synechocystis* sp. PCC 6803 colonies on the top layer of the photobioreactor were monitored for three weeks via fluorescent microscopy. **(b)** Increase in average algae surface coverage density over time. Fluorescent images of algae on the surface of the waveguide were taken at three different locations along the length of the photobioreactor and were used to calculate average surface coverage density through image analysis (See Methods).

To demonstrate the spatial uniformity of biomass accumulation in the bioreactor (indicative of even light distribution) *Synechocystis sp.* PCC 6803 2x EFE (Ungerer et al., 2012) was cultured in the 10-stack photobioreactor for three weeks. This strain of algae was genetically modified by another lab (Ungerer et al., 2012) to produce ethylene and was used as a model organism in this study. The waveguides in the photobioreactor were optically activated by red light ($\lambda \sim 630$ nm) from LEDs coupled into the ends of waveguides on both side of the photobioreactor. The entire culture medium was exchanged daily via tubes that were individually connected to each of the ten layers. Flow rate of fresh media was low enough to keep changes in the distribution of algae on the surface minimal. After inoculating the bioreactor with *Synechocystis*, growth was monitored for three weeks by measuring the fluorescent intensity of the *Synechocystis* colonies on the top layer of the photobioreactor via a fluorescent microscope.. Fluorescent images taken at

three different locations along the length of the bioreactor were analyzed using the methods described in Materials and Methods. The initial base line surface coverage density after initial inoculation of the bioreactor with the *Synechocystis* was measured to be 1.4%. The surface density increased uniformly across the waveguide surface, and reached up to 93% on day 9 (**Figure 4.2(b)**). The standard deviation of the surface coverage was within 5%, indicating uniform growth rates regardless of location of the algae on the waveguide. The uniform growth patterns were indicative of an even distribution of light over the waveguide, demonstrating an effective utilization of the entire surface by the algae culture.

4.4.3 Light distribution in the ten-stack photobioreactor

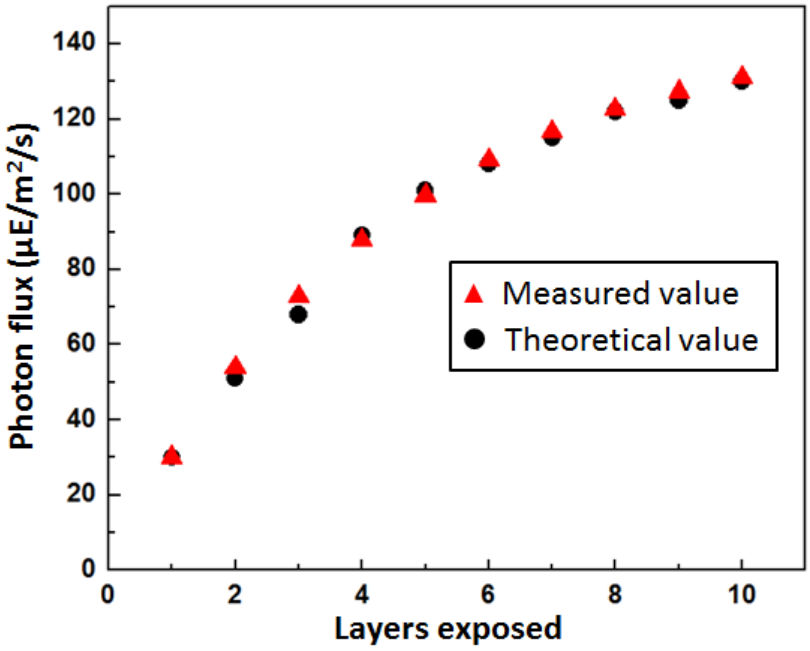

FIGURE 4.3 Light Intensity Distribution in the Ten-Stack Photobioreactor: Measured (red triangles) and modeled (black dots) light intensity from the top layer of the ten-stack photobioreactor as a function of the number of layers exposed. The strong agreement of the measured values with the theoretical calculations indicates that the light emanating from each waveguide was the same, irrespective of the location of the waveguide in the ten-stack reactor.

The light emanating from the waveguide in each layer of the stack was quantified to determine the distribution of light within the photobioreactor. Due to the inaccessibility of the inner layers for measurement of light intensity, the light distribution was quantified on the basis of the measurements over the top layer. It should be noted that in an empty bioreactor the measurement over the top most layer includes contributions from all the layers below. To quantify the contribution of each layer to the measurement at the top layer, each layer was exposed in sequence and measured the intensity at the top. The measurement was repeated for all ten layers, starting from the top layer and sequentially adding lower layers (*i.e.* only the top layer was exposed in the first measurement and all of them in the last measurement). As anticipated, all the layers contributed to the intensity measured at the top, with decreasing contribution from lower layers (**Figure 4.3**). This can be attributed to a constant loss of intensity as the light passed through an increasing number of etched glass slides above.

Under the assumptions that (1) the intensity of light emanating from each waveguide layer is the same, and (2) there is a certain (fixed) percentage loss as that light passes through each additional layer, the expression for the amount of total light intensity seen at the top most layer can be calculated to be:

$$I(n) = \mathrm{a} * \frac{1-(1-\mathrm{r})^{\mathrm{n}}}{1-(1-\mathrm{r})} \qquad (1)$$

Where *I(n)* is the light intensity at the top when *n* layers of the stack are exposed, *a* is the uniform light intensity emanating from each layer, and *r* is the fraction of light that is lost as it passes through one waveguide layer above. For *a* =30 (the intensity as measured from only the top layer) and *r*~0.205, the formula above fits well with the experimental curve (**Figure 4.3**).

The fit between the experimental and the theoretical curve therefore supports the assumption that the light intensity from each waveguide is the same.

4.4.4 Increased biomass production

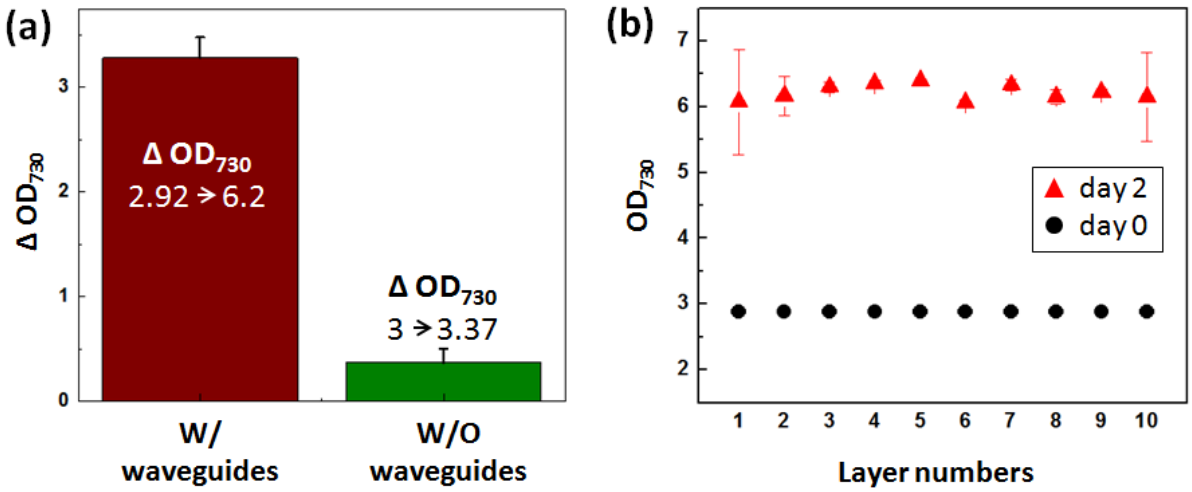

FIGURE 4.4 Biomass Accumulation in the Ten-Stack Photobioreactor :(a) Comparison of biomass accumulation (change in OD_{730}) in photobioreactors with and without internal waveguides (IW). *Synechocystis* sp. PCC 6803 2x EFE algal strain was cultured for two days in both photobioreactor types. After two days of illumination by red light (630 nm) at an intensity of 10 µE m^{-2} s^{-1}, the average OD_{730} increased from 2.92 to 6.2±0.18 in photobioreactors with IW (red bar) while the OD_{730} increased from 3 to 3.37±0.1 in photobioreactors without IW (green bar). **(b)** Increase of OD_{730} across each of the ten layers of the ten-stack photobioreactor. The *Synechocystis* sp. PCC 6803 was cultured for two days in the ten-stack photobioreactor and the culture was individually extracted from each of the ten layers. Black circles and red triangles represent the OD_{730} of algal solutions from ten layers measured on day 0 and day 2, respectively. Note that similar growth was obtained across all ten layers.

Biomass production within the bioreactor was quantified by comparing the 10-stack bioreactor with an identical control bioreactor which did not contain any internal waveguiding structures. For these experiments, all photobioreactors were inoculated with the *Synechocystis* sp. PCC 6803 solution at OD_{730} ~3 and were operated at the same incident light intensity (10µE m^{-2} s^{-1}) measured over the surface of the top layer waveguide. To eliminate the effect of free space

optical coupling in the bioreactor without waveguides, the incident light was first coupled into external waveguides (*i.e.* short glass slides inserted 3mm deep into both side of the bioreactor) and then distributed into the bioreactor. Experiments were repeated in triplicate for both the experiment and the control photobioreactor. After two days of continuous illumination with red light, the average OD_{730} increased from 2.92 to 6.2±0.18 in photobioreactors with integrated waveguides while only a slight increase, from 3 to 3.37±0.1, was observed in the control photobioreactors (**Figure 4.4(a)**). The average biomass production rate of the bioreactor with the waveguides was therefore 8.6 times higher than the control bioreactor.

Uniformity of biomass accumulation along the height (stack-wise) dimension of the bioreactor was examined by comparing biomass accumulation in each of the ten stacks. In these experiments each bioreactor stack was inoculated with the *Synechocystis* strain and was allowed to grow for two days under an incident light intensity of 10μE m^{-2} s^{-1} (emitted from the surface of each waveguide). Illumination was continued for two days and the cultures were extracted from each of ten stacks. The experiment was repeated in triplicates for each of the two types of bioreactors. Over two days, OD_{730} of the *Synechocystis* solutions in each layer changed from 2.92 to 6.2 on average (**Figure 4.4(b)**). The variation of the OD_{730} change between separate layers was small, with a standard deviation of 0.136, demonstrating good uniformity in biomass production.

4.4.5 Ethylene production

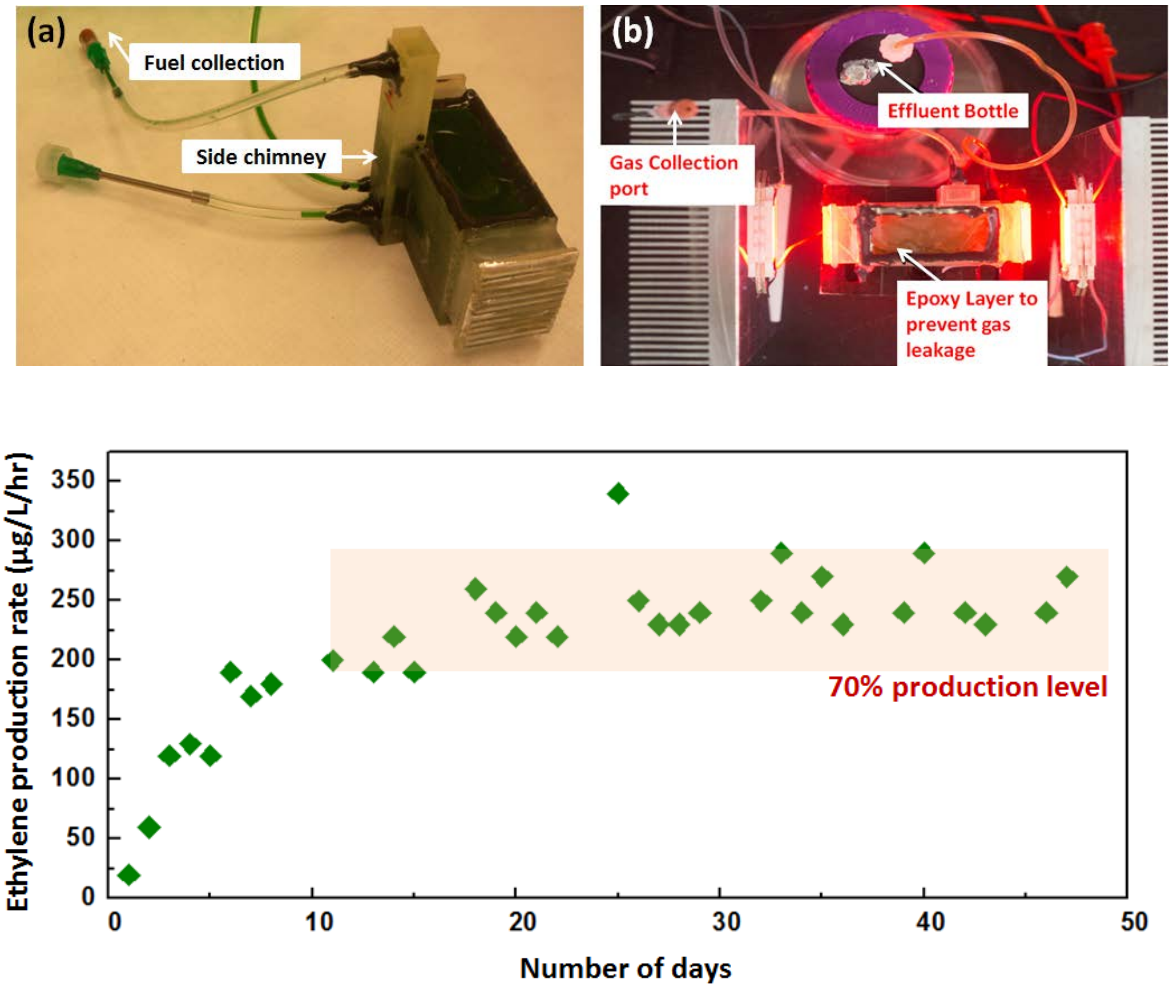

FIGURE 4.5 Design of the Ten-Stack Photobioreactor for Ethylene Production (a) Modified bioreactor design for ethylene collection – the addition of the side chimney enabled easier collection and extraction of the gaseous fuel product from the bioreactor **(b)** Experimental setup with side coupled LEDs. The effluent bottle was used to collect liquid culture displaced by the secreted gaseous products. **(c)** Ethylene production by *Synechocystis* sp. PCC 6803 within the ten-stack photobioreactor for over 45 days. After an initial growth period, the culture density was maintained constant at OD_{730} ~9.

After demonstrating improved growth rates in the stacked photobioreactors, the bioreactor design was modified for collection of ethylene produced by *Synechocystis* sp. PCC 6803 2xEFE (Ungerer et al., 2012). To minimize leakage of ethylene from the stacked bioreactors, they were

fortified with a coat of parylene, which reduces gas permeability, and the number of entry/exit ports from one for each layer was reduced to one entry/exit for the entire bioreactor. This was accomplished by introducing a side "chimney" to the bioreactor, which connected all layers of the bioreactor to each other (**Figure 4.5 (a) and (b)**). Other design and fabrication aspects of the bioreactor remained as described in Methods.

Experiments were carried out in the modified bioreactor to demonstrate growth of the algal culture from a low OD and to measure ethylene production. An inoculum of OD_{730} ~1 was extracted from a high-density culture (see Methods), and used to inoculate the modified 10-stack bioreactors. The bioreactors were illuminated from the sides by red LEDs ($\lambda \sim 630$ nm), as before. Carbon was provided through carbon enriched media (see Methods). When the culture was illuminated, the algal culture secreted gaseous products which could be visually perceived as gas bubbles, increasing in number and volume over time. To trap the gas for collection and subsequent analysis, the output port on top of the chimney was kept closed via a rubber septum, while the influent port at the lower edge corner of the bottom layer was kept open and connected to a sterile bottle for collection of the effluent culture pushed out due to the increased pressure in the bioreactor due to the gaseous products. The photobioreactor design allowed the buoyant forces to push the gas products to the top of the chimney (port closed) while only liquid effluent was displaced during operation, ensuring minimal loss of gaseous products from the photobioreactor. After gas collection and analysis from the bioreactor (see Methods), the liquid culture was extracted from the bioreactor, centrifuged, and resuspended in fresh medium. This experiment was carried out for over 45 days after starting with an initial culture of $OD_{730} \sim 1$.

The ethylene production rate increased from an initial value of 0.02 mg L^{-1} h^{-1} on day 1 to approximately 0.2 mg L^{-1} h^{-1} on day 10 (**Figure 4.5(c)**), corresponding to a growth of the culture within the bioreactor from OD_{730} of 1 to an OD_{730} of 9. To demonstrate that consistent production rate of ethylene can be maintained in these bioreactors, the optical density of the culture was controlled at an OD_{730} of 9 for the remainder of the experiment. At each resuspension the grown culture was diluted to OD_{730} of 9. This experiment was repeated daily for over 45 days and production rates remained within a window of approximately 70% of the maximal production rate for over 35 days (**Figure 4.5(c)**), demonstrating that the stacked bioreactors are suitable for consistent production of fuel over long periods of time, a necessary requirement for any biofuel production system.

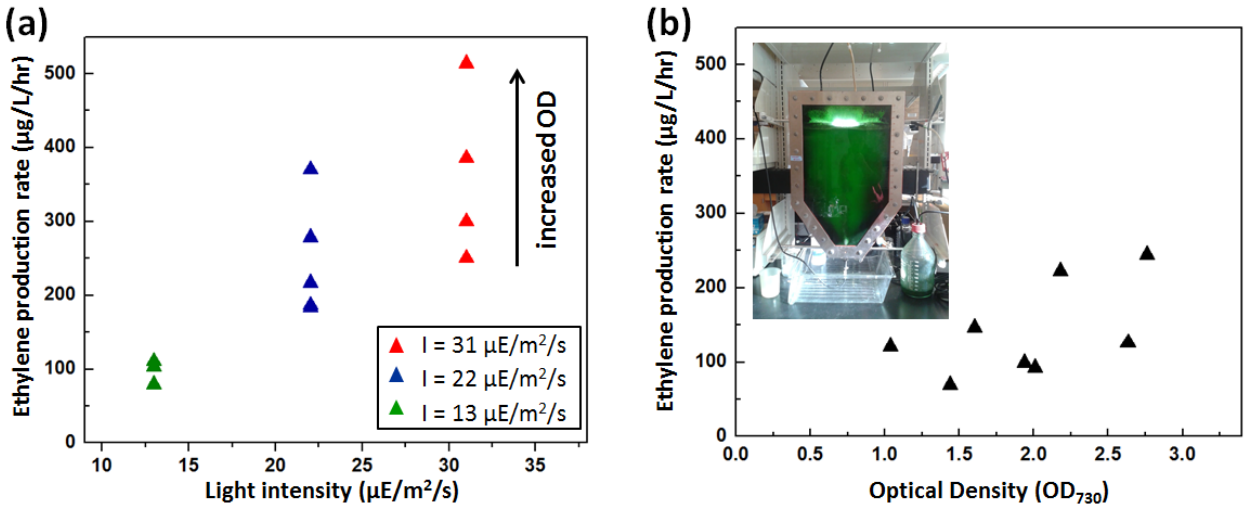

FIGURE 4.6 Ethylene Volumetric Productivity and Comparison with Conventional Photobioreactor: (a) Increase in ethylene production rates with increase in light intensity in a ten-stack photobioreactor. The maximal production rate reached up to 0.510 mg L^{-1} h^{-1}. (b) Production rates as measured from the conventionally run flat plate bioreactor (Inset). The maximal production rate was 0.244 mg L^{-1} h^{-1} - less than half of that achieved in the stacked photobioreactor.

The volumetric productivity of the stacked bioreactor was further improved by modifying the light intensity incident from the waveguides. The experiments were carried out as described before, with an initial inoculum of OD_{730} ~ 6 allowed to grow at a fixed light intensity. The experiment was carried at three different intensities – 13, 22 and 31 μE $m^{-2}s^{-1}$(as measured emanating from each waveguide) and ethylene production was measured (see Methods). The production rates considerably increased as the light intensity was increased with production rates reaching as high as 0.51 mg L^{-1} h^{-1} at intensities of 31 μE m^{-2} s^{-1} (**Figure 4.6(a)**). This also corresponded to growth of the culture from an initial OD_{730} of 6 to a final OD_{730} of 11.

4.4.6 Comparison with a flat plate photobioreactor

A conventional flat plate bioreactor was assembled with a light path of 3 cm (see inset in **Figure 4.6(b)**) and operated to establish a benchmark for the volumetric productivity of a conventional photobioreactor. Details of operation of the flat plate bioreactor are provided in the Materials and Methods section. The production rates for the flat-plate bioreactor were measured (**Figure 4.6(b)**). The light path of 3 cm in the flat plate photobioreactor (compared to the 2 mm path length in the 10 stacked photobioreactors) led to considerable self-shading, despite active mixing of the algal culture in the photobioreactor. This prevented the biomass from achieving a higher density than OD_{730} of 2.8. At the observed OD_{730} between 1 and 2.8, the measured ethylene production was between 0.069 mg L^{-1} h^{-1} and 0.244 mg L^{-1} h^{-1} with a considerable variance in production rates. This variability in production rates can be attributed to sparging differences leading to varying mixing conditions, and possible sampling errors. Regardless, the volumetric productivity of the ten-stacked photobioreactors was at least twice as high as that of a conventional flat-plate bioreactor despite the higher light intensity for the flat-plate bioreactor

(200 µE m^{-2} s^{-1}). Further, the 10-stack bioreactors were shown to support denser cultures, up to OD_{730} of 11, compared to OD_{730} of ~3 supported by the flat-plate bioreactor.

4.4.7 Implication of the Stacked Photobioreactor design

Light distribution is one of the primary factors determining the productivity of algal photobioreactors (Zittelli et al., 2013). Growth of high-density cultures in traditional photobioreactors, which is a key prerequisite for high volumetric productivities, is not possible due to the short penetration depth of light. In conventional systems this limitation is alleviated by various mixing strategies in which the culture is circulated across the light gradient to ensure that the algae are on average exposed to sufficient light. This is inherently energy intensive, leading to low EROIs, and have been estimated to be as much as 1/3rd of the whole energy cost in the growth, extraction, and production of algae biofuel (Beal et al., 2012a). As demonstrated by the results above, the ten-stack photobioreactor design inverts the paradigm of bringing algae to the illuminated regions, by bringing the light directly to the algae, which was, in the above experiments, maintained as a static culture. The high surface-to-volume ratios in the stacked bioreactors with the short light paths ensure that sufficient light penetration is achieved even with ultra-dense cultures. Although high surface area would require increased material and capital costs in a scaled up plant, this could be minimized by employing thinner waveguides (~100 microns) and thus increasing the ratio of the working volume of the bioreactor to the material volume. By employing improved dimensions for waveguides (say 1m x 0.2m x 150 µm, with a 2 mm spacing between stacks), we can, for example, reduce the material volume (of the waveguides) to 7.5% of the liquid volume. We believe these extra costs can be offset by the capital costs saved by reduced requirement of land, and more importantly by the savings in operational costs afforded by the design of the stacked waveguide photobioreactor.

In addition to the improved growth and volumetric production rates, the ten-stack photobioreactors developed have other design features that are attractive for algal biofuel production. The stackable architecture of the stacked photobioreactors leads to reduced requirement for land usage. Further, since optical fibers can be used to transport collected sunlight and subsequently couple light into the integrated waveguides, it is possible to physically separate the collection of solar incidence from the operation of the bioreactor. This allows for deployment of these photobioreactors in settings that might not traditionally be environmentally possible (*e.g.* cold/hot weather locations or urban settings). The ultracompact nature of the bioreactor also opens the possibility of having a portable biofuel production plant.

4.5 Conclusion

A 3D stackable waveguide photobioreactor that aims to alleviate poor distribution of light within conventional photobioreactors, was demonstrated. The approach of using closely stacked slab waveuides enabled uniform distribution of light within the bioreactor leading to an eight-fold increase in biomass growth compared to a control bioreactor. The ten-stack photobioreactor was also capable of supporting consistent production of ethylene over 45 days, demonstrating its suitability for biofuel production over long periods of time. It also improved the ethylene volumetric productivity two fold over a conventional photobioreactor. These results demonstrate the efficacy of the design, encouraging further investigation for full scale development.

CHAPTER 5

DETERMINATION OF OPTIMAL INTENSITY AND CARRYING CAPACITY OF A THIN LIGHT PATH PHOTOBIOREACTOR

Adapted from: Aadhar Jain[‡], Nina Voulis[‡], Erica E.Jung, Devin D.R. Doud, William Miller, Largus T. Angenent, and David Erickson. In preparation for Environmental Science and Technology

‡Both authors contributed equally to the work

5.1 Abstract

Production of competitive microalgal biofuels requires development of high volumetric productivity photobioreactors (PBRs) capable of supporting high density cultures. Carrying capacity of current PBRs is limited by non-uniform distribution of light due to self-shading effects. We recently developed a thin light path stacked photobioreactor (S-PBR) with integrated slab waveguides which resolves this issue. In the present work we enhance the performance of the S-PBR by determining the optimal wavelength and intensity regime of the incident light. This enables the S-PBR to support high density cultures, achieving a carrying capacity of OD_{730} 20. Using a genetically modified algal strain capable of secreting ethylene, we improve ethylene production rates to 937 μg L^{-1} h^{-1}. This represents a near twofold improvement over production rates achieved in earlier work, and a fourfold improvement over a conventional flat plate PBR. These results demonstrate the advantages of the S-PBR design and provide the optimal operational parameters to maximize volumetric production.

5.2 Introduction

Driven by the need for sustainable alternatives for fossil fuels, energy research today is focused on a range of renewable resources, including biomass. Algae are of particular interest as a sustainable feedstock for transportation fuel due to their salient advantages over terrestrial crops, including higher area yields(Chen et al., 2011; Yusuf, 2007; Zhao et al., 2013), smaller water footprint, ability of certain strains to grow in brackish or saline water, and applicability of waste streams as a low-cost source of CO_2, nitrogen and phosphorus(Greenwell et al., 2010; Mata et al., 2010; Pires et al., 2012; Posten and Schaub, 2009; Rodolfi et al., 2009; Wijffels and Barbosa, 2010; Yun et al., 1997). Besides biofuels, algae cultivation is also used for production of food and feed supplements(Janssen et al., 2003; Wijffels et al., 2010), showing the versatility of algal products and further encouraging the development of high efficiency photobioreactors (PBRs).

Current commercial algae cultivation relies on open ponds, primarily due to low capital costs(Greenwell et al., 2010; Johan U Grobbelaar, 2008; Wijffels and Barbosa, 2010). This technology however has a number of disadvantages if used for large-scale production of bulk commodities such as biofuel(Johan U Grobbelaar, 2008; Ogbonna et al., 1999). These shortcomings include low biomass densities(Greenwell et al., 2010; Posten and Schaub, 2009; Wijffels and Barbosa, 2010), requirement of large surface areas, contamination(Ogbonna et al., 1999; Rodolfi et al., 2009), incompatibility with cultivation under atmosphere with elevated CO_2 levels(Posten and Schaub, 2009), and high water losses due to surface evaporation(Posten and Schaub, 2009).

Production of high-volume commodities therefore requires growth systems to overcome these limitations through deployment of alternative technologies such as closed PBRs(Johan U

Grobbelaar, 2008). Although conventional closed PBRs (*e.g.* flat-plate and tubular reactors) enable algae cultivation in more controlled environments than open ponds, they still suffer from suboptimal light distribution(Grobbelaar, 2010; Janssen et al., 2003; Yusuf, 2007). Under standard operation regimes, algae close to the illuminated surface are photoinhibited, while algae in the interior of the reactor are photolimited(Brennan and Owende, 2010; Carvalho et al., 2011; Grima et al., 1996; Johan U Grobbelaar, 2008; Kunjapur and Eldridge, 2010; Long and Humphries, 1994; Richmond et al., 2003). These effects are mitigated by employing mixing strategies which circulate the algae cells across the light gradient, thus ensuring an adequate average light exposure(Aci??n Fern??ndez et al., 1999). However, the energy requirements for mixing are high, amounting even in simple systems to 3 W m^{-2}, close to the energy eventually harvested from algal biomass(Posten and Schaub, 2009) and contributing to overall energy efficiency ratios of less than one(Beal et al., 2012; Jegan et al., 2014). Mixing also accounts for 13% to 52% of total construction and operation costs of conventional closed PBRs(Norsker et al., 2011).

In an earlier publication(Jung et al., 2014) we addressed the limitations posed by simultaneous photoinhibition and photolimitation in conventional closed PBRs. We embraced a holistic PBR design by (1) delivering light through optical waveguides for optimal light distribution inside the reactor, (2) aiming for dense cultures facilitating high volumetric product yields, and (3) envisaging utilization of product-secreting algae. The latter would simplify post-processing steps and avoid costly and technically challenging harvesting and product extraction steps(Kleinegris et al., 2011), which can contribute up to 50% of the total product cost(Greenwell et al., 2010).

To achieve this, we have demonstrated a short light-path stacked photobioreactor (S-PBR) with internal light distribution through optical slab waveguides. Incident light is coupled into the sides

of each slab waveguide and is propagated along the length of the waveguide via total internal reflection. The surface of the optical waveguide is etched to create randomly distributed refractive index changes, thus disrupting the propagating light wave and releasing the light into the bioreactor volume. Combined with short light-paths (~1 mm), the waveguides enable the delivery of optimal light intensities throughout the entire volume of the S-PBR, avoiding both photolimitation and photoinhibition as well as reducing the need for energy intensive and costly mixing. The resulting 3D architecture both reduces the amount of land area required and supports high density cultures, leading to a high areal productivity. In the S-PBR we showed an eightfold higher biomass accumulation than achieved in a control PBR without optical waveguides(Jung et al., 2014).

Aiming to avoid costly cell-harvesting steps, we used a product-secreting *Synechocystis* sp. PCC 6803 2x EFE. This algae strain had been genetically modified to secrete the biofuel precursor ethylene(Ungerer et al., 2012). Using the S-PBR, we had demonstrated consistent production of ethylene for over 45 days. We had achieved a two-fold increase in volumetric ethylene production rates as compared to a flat-plate PBR. The earlier achieved results validate the design and performance of the S-PBR, indicating its promise as a viable photobioreactor technology. In this work, we explore methods to further improve yields and energy efficiencies. We optimize production over wavelength and intensity of the supplied light.

Photoautotrophic algae preferentially use certain wavelengths in the photosynthetic active radiation (PAR) range, depending on the collection of light harvesting pigments present in their photosynthetic machinery(Carvalho et al., 2011). Chlorophyll constitutes the most important group of these pigments and absorbs in the blue (450-475 nm) and the red spectral range (630-675 nm)(Carvalho et al., 2011; Grobbelaar, 2010). Excitation of a chlorophyll molecule in the

reaction centers of photosystem I and II requires energy equivalent to that contained in photons with a wavelength of 700 and 680 nm respectively(Carvalho et al., 2011). Algae should therefore be supplied with light in the red spectral range to minimize energy dissipation. The efficacy of algal production under red light has been previously shown by multiple studies (Gordon and Polle, 2007; Katsuda et al., 2004; Matthijs et al., 1996; Wang et al., 2007; Zhao et al., 2013).

Besides wavelength, intensity of the supplied light is another important parameter determining algal growth. The optimum intensity for many algal species lies in the range of 100 to 400 $\mu E\ m^{-2}\ s^{-1}$ (Carvalho et al., 2011; Posten and Schaub, 2009; Wijffels et al., 2010). Photolimitation occurs at lower light intensities, when insufficient photons are available to carry out photosynthesis at the rate required for optimal cell growth. Photoinhibition on the other hand leads to cell damage induced by high light intensities, adversely affecting growth(Carvalho et al., 2011). While algal growth, thus, follows a concave function with respect to intensity, photosynthetic efficiency (PE) decreases with increasing intensities as photosynthetic centers become more saturated(Carvalho et al., 2011; Fan et al., 2008; Gordon and Polle, 2007). Therefore, design of algal production systems needs to account for both the optimal growth window and sufficient PE(Cheirsilp and Torpee, 2012; Gordon and Polle, 2007; Li et al., 2012; Ruangsomboon, 2012; Sorokin and Krauss, 1958; Zhao et al., 2013).

In the following we first report the effects of variation of wavelength and intensity of the supplied light on ethylene production rates of *Synechocystis* sp. PCC 6803 2xEFE. Secondly, we investigate the effect of high density culture on ethylene production rates to determine the carrying capacity of the S-PBR. Finally, using the collected data, we determine the photosynthetic efficiencies achieved in the present system. The results provide us with optimal illumination conditions and biomass densities to maximize ethylene production in the S-PBR.

5.3 Materials and Methods

5.3.1 Stacked Photobioreactor Design and Assembly

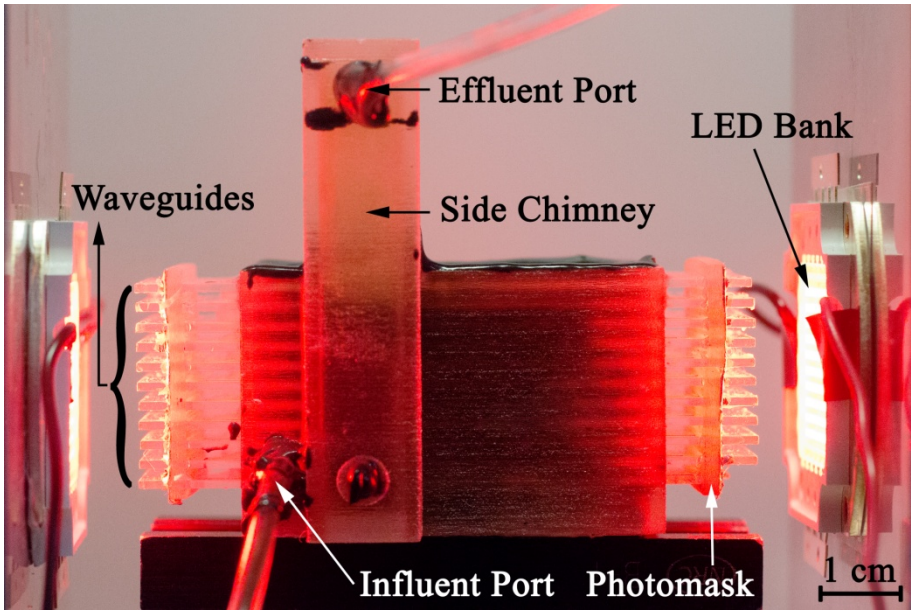

Figure 5.1 Ten-stack 3D printed photobioreactor in operation. The reactor is illuminated from each side by red (630 nm) LED banks. The light is coupled into the waveguides, which transport and evenly distribute the light inside the reactor. The photomask prevents uncoupled light from entering the reactor. The side chimney connects the layers and allows collection of the produced gas. The influent port is used to inoculate the reactor before operation and collect displaced liquid during operation. The produced gas is extracted through the effluent port.

The S-PBR consisted of a 3D frame with slots to stack slab waveguides vertically above each other. The dimensions of the S-PBR were 7.5 cm x 2.5 cm x 3 cm (length x width x height) with a 2-mm gap separating two waveguides, and a total liquid volume of 16 mL. The S-PBR had two ports: (1) bottom influent port for inoculation and (2) top effluent port for gas product removal (**Figure 5.1**).

The frame was 3D printed from a photocurable resin (VeroClear, Stratasys Ltd, Edina, Minnesota, United States). It was coated by Parylene C via a vapor deposition process to reduce gas permeability of the S-PBR. The waveguides were placed into dedicated slots in the frame

and fixed to the frame by using Polydimethylsiloxane (PDMS) (Dow Chemicals, Midland, Michigan, USA) as a resin. This also ensured that any gaps (due to manufacturing errors in the 3D printing process) between the frame and the waveguides were sealed by the cured PDMS. Since PDMS is gas permeable, the assembled reactor was subjected to a second coat of Parylene C to ensure gas impermeability. To prevent uncoupled light from entering the S-PBR, the gaps between the slab waveguides were covered by a photomask (printed from the same photocurable resin as the frame). Aluminium foil was attached to the photomask to improve reflectance characteristics.

5.3.2 Waveguide Fabrication

The S-PBR waveguides were fabricated by affixing thin cover slips (VWR Micro Cover Glasses) to chemically etched borosilicate microscope slides (VWR VistaVisio Microscope Slides, Radnor, Pennsylvania, USA). Glass etching paste (Armour Etch, Hawthorne, New Jersey, USA) was applied on the glass slides for seven hours, and subsequently washed away, creating randomly distributed surface defects for improved light scattering from the waveguide surface. The thin coverslips were attached on top of each glass slide using uncured PDMS as a resin and curing the assembly for two hours at 80°C. Attaching a coverslip on top of the glass slide increased the intensity of light scattering due to higher index contrast between the core and the cladding of the waveguide(Jung et al., 2014), *i.e.* by changing the refractive index of the medium adjacent to the glass slides from 1.33 (water) to 1(air).

5.3.3 Model organism

The model organism in all experiments was *Synechocystis* sp. PCC 6803 2x EFE. This genetically modified strain was selected due to its ability to secrete ethylene, a biofuel precursor, as a gaseous product(Ungerer et al., 2012). Prior to inoculation, algal cultures were grown in semi-batch in gastight 1 L reactors with 20 mL liquid phase at 30°C and continuous broad spectrum illumination (100 µE m^{-2} s^{-1}). The culture was grown in fivefold concentrated BG-11 augmented with 25 mg L^{-1} spectinomycin, 200 mg L^{-1} kanamycin and 4.6 g L^{-1} TES buffer. Carbon was provided both via the gaseous phase (5% CO_2 atmosphere) and via the liquid medium (20 mM $NaHCO_3$). These conditions allowed long term steady-state maintenance of a dense algal culture at an OD_{730} of 60. Aliquots were taken from the semi-batch culture and, after dilution in growth medium to the required density, used as inoculum for the S-PBR.

5.3.4 Experimental Setup and Procedure

The S-PBR was inoculated at a starting OD_{730} of 10 (at 470, 630 and 660 nm), 20 (at 630 nm), and 30 (at 630 nm). The bioreactors were illuminated from each side via an LED bank of the specified wavelength (630 nm or 660 nm) and at five levels of intensity (35, 52, 69, 86, and 104 µE m^{-2} s^{-1}). The incident light was coupled into the waveguides, propagated along the length of the waveguides and subsequently emitted to the algal culture by the scattering surface on the waveguides. During the course of each experiment the bioreactor influent port was connected to a sterile bottle for collection of the displaced culture volume, while the effluent port on top of the side chimney was sealed by a septum to retain the secreted gaseous products in the S-PBR.

On illumination by the LED bank, the algal culture grew and secreted gaseous products (including ethylene) as a result of the photosynthetic process. The formed gas bubbles displaced equal volume of culture through the effluent port into the sterile effluent bottle. The design of the side chimney ensured that the secreted gaseous products were separated from the liquid volume and could therefore be easily extracted.

At the end of the experimental run, the gaseous products were extracted from the S-PBR and analyzed. Subsequently, the whole culture volume was removed from the bioreactor, centrifuged and subsequently resuspended in fresh medium. After two experimental runs in which the algae acclimatized to the new culture conditions, the procedure was repeated multiple times for each combination of density, incident light wavelength and intensity. A new inoculum, taken from the semi-batch culture, was used to inoculate the S-PBR for each new combination of experimental conditions.

5.3.5 Gas Extraction and Analysis

Gaseous products were extracted from the bioreactor upon completion of each experimental run. As the gas was removed through the septum at the effluent port, the liquid culture displaced earlier into the connected bottle was simultaneously pulled back into the bioreactor through the influent port. This prevented any dilution of the gaseous sample by the ambient air. The concentration of ethylene in the samples was analyzed using a gas chromatograph (GC). (See analysis procedure in earlier work(Jung et al., 2014).)

5.3.6 Measurement of Light Intensity

Due to inaccessibility of the waveguides (except the top one) within the S-PBR, it was not possible to measure the light emanating from each individual waveguide. However, our previous work(Jung et al., 2014) had established that the intensity distribution within the S-PBR was uniform across layers and contributed to the measurement made over the top waveguide. This could be therefore be used to estimate the light intensity emanating from each waveguide by a single measurement over the top waveguide. From previous work(Jung et al., 2014), it was found that the intensity at the top was given by:

$$I(n) = \mathrm{a} * \frac{1-(1-\mathrm{r})^{\mathrm{n}}}{1-(1-\mathrm{r})} \qquad (5.1)$$

Where *I(n)* is the light intensity at the top when *n* layers of the stack are exposed, *a* is the uniform light intensity emanating from each layer, and *r* is the fraction of light that is lost as it passes through one waveguide layer above. By fitting the measured data to the expression above the value of *r* was established experimentally to be 0.205. For this value of *r*, Equation (1) can be inverted to find the light intensity emanating from each waveguide as

$$\mathrm{a} = 0.227 * I(10) \qquad (5.2)$$

where *I*(10) is the intensity measured over the top waveguide when all 10 layers are exposed. Thus, we measured the intensity over the top waveguide of an empty reactor and used equation (2) above to estimate the light intensity from each individual waveguide.

5.3.7 Statistical Data Analysis

Statistical analysis on the collected data was performed using the software package R(R Core Team, 2014). Separate general linear regression models were fit for ethylene production rates and PE of ethylene production. In both models, illumination wavelength, intensity and culture OD were used as independent variables. The overall family-wise error rate (FWER) was controlled at 5% using R multivariate marginal models (mmm) package. The results of the regression analysis can be found in Supplementary Information (SI). The optimal values of OD and intensity for ethylene production were calculated assuming a multiplicative interaction term between OD and intensity. Standard errors (SE) for the optimal values were calculated using the simplified variance formula(Ku, 1966).

5.4 Results

5.4.1 Ethylene Production Rate Dependence on Light Wavelength and Intensity

Experiments were conducted to evaluate and quantify the effect of wavelength and intensity of the incident light on the ethylene production rates of the genetically engineered strain of algae S. PCC 6803 2x EFE in the S-PBR. The tested wavelengths of the incident light were chosen to target the absorbtion peaks of the pigment chlorophyll - in red and blue spectrum of visible light – with experiments conducted at red (630 nm), deep red (660 nm) and blue (470 nm) wavelengths. Experiments could not be conducted at the peak situated around violet (~430 nm) due to the unavailability of a suitable illumination source at that wavelength. Experiments were carried out at five intensity levels with a culture of OD_{730} 10. Experiments at blue (470 nm)

wavelength were discontinued after ethylene production was found to be negligible (results not shown).

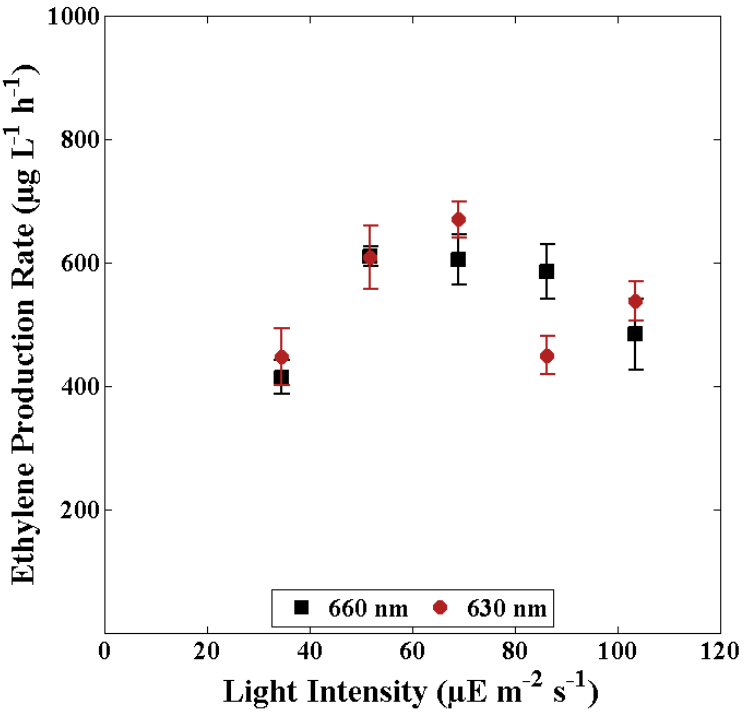

Figure 5.2 Volumetric ethylene production rates in the S-PBR achieved by *Synechocystis* PCC 6803 2x EFE algal strain (OD_{730} of 10) in the S-PBR. The figure shows results obtained at two different wavelengths (630 nm and 660 nm) and five light intensity levels (35 μE m^{-2} s^{-1} to 104 μE m^{-2} s^{-1}). The flags indicate standard errors.

Ethylene production rates measured for each of the intensities at red (630 nm) and deep red (670 nm) are shown in **Figure 5.2**. Ethylene production rates were dependent on light intensity, with maximum production at 69 μE m^{-2} s^{-1} for both red and deep red illumination. The concave nature of the curve (p-value < 0.001, see SI) suggests that at lower intensities the algae were photolimited due to the dominant shading effects, while at high light intensities the ethylene production decreased due to photoinhibition. However, there was no statistically significant

difference between the red and the deep red illumination sources indicating that the algae were capable of utilizing either of the wavelengths equally efficiently.

5.4.2 Ethylene Production Rate Dependence on Culture (OD_{730})

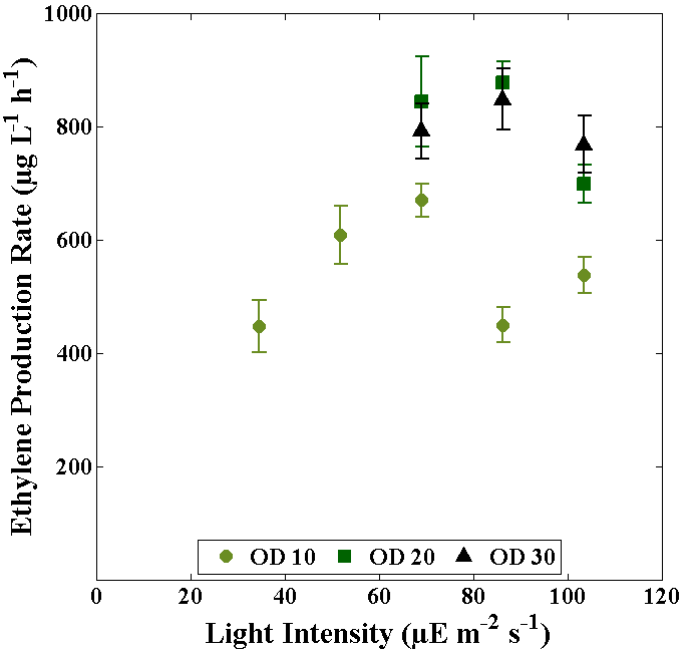

Figure 5.3: Volumetric ethylene production rates in the S-PBR achieved by *Synechocystis* PCC 6803 2x EFE algal strain at 630 nm. The figure shows results obtained at three different culture densities (OD_{730} of 10, 20 and 30) and five light intensity levels (35 µE m^{-2} s^{-1} to 104 µE m^{-2} s^{-1}). The flags indicate standard errors.

We hypothesized that the short light path (1 mm) in the S-PBR should be capable of supporting considerably higher densities of algae culture and thus further increasing the volumetric production rates. Experiments were therefore conducted with higher density algal cultures at OD_{730} 20 and OD_{730} 30. Since the earlier experiments indicated no significant difference between red and deep red illumination sources, experiments with high culture densities were only carried

out with the red (630 nm) light source. Three levels of light intensity were tested to determine the optimal operation point at high culture densities (**Figure 5.3)**.

The maximal ethylene production rate for the OD_{730} 20 was nearly 30% higher - 937 µg L^{-1} h^{-1} as compared to 715 µg L^{-1} h^{-1} observed for OD_{730} 10 culture, demonstrating that the S-PBR was capable of supporting high culture densities. The maximal production rate for OD_{730} 20 was found at intensity of 86 µE m^{-2} s^{-1}. This is higher than that observed for OD_{730} 10 (69 µE m^{-2} s^{-1}), which is indicative of a greater shading effects in the denser culture.

A similar functional dependence on light intensity was observed for OD_{730} 30, although the production rates were lower than those for OD_{730} 20, but greater than those for OD_{730} 10 (p-value < 0.001) (**Figure 5.3**). Moreover, at OD_{730} 30 the culture density decreased (data not shown) over the course of the experiment, suggesting that light attentuation due to absorbtion by the algae was too significant to penetrate even through the small 1-mm light path. This indicates that the maximum carrying capacity of the S-PBR, with a 2-mm spacing between the stacks, lies between an OD_{730} 20 and OD_{730} 30 (equivalent to cell dry weight (CDW) of 9 - 14 g L^{-1}).

5.4.3 *Photosynthetic Efficiency*

Besides volumetric productivity, another important consideration is the PE exhibited by the algae inside the S-PBR. PE is defined as the ratio of the amount of energy stored by the algae to the amount of photon energy absorbed. PE can be defined in terms of (1) total biomass produced, or (2) product, *i.e.* ethylene, secreted. In both cases, as a conservative assumption, the entire light

incident on the algae (*i.e.* the light emanating from the surface of an individual waveguide) was assumed to be absorbed completely.

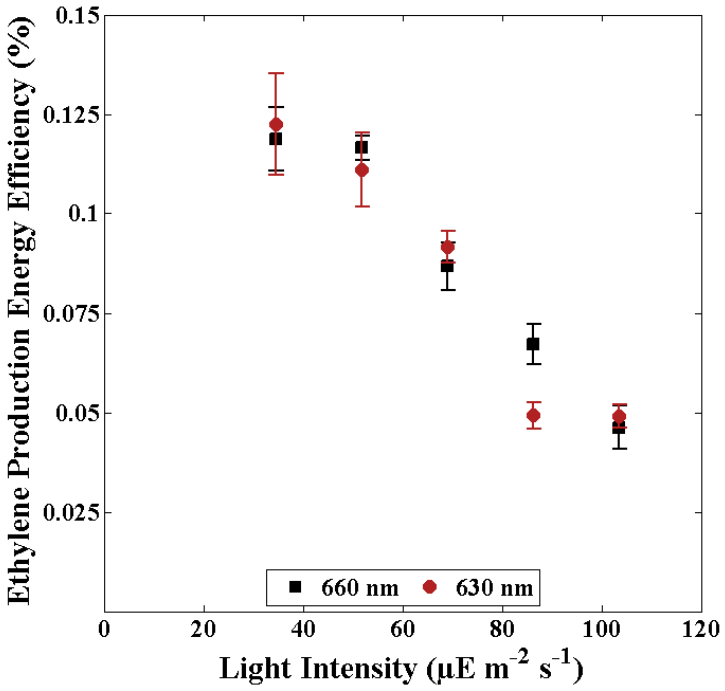

Figure 5.4 Conversion efficiency from light incident on the algal culture to energy contained in ethylene secreted by *Synechocystis* PCC 6803 2x EFE (OD_{730} 10). The figure shows results obtained at two different wavelengths (630 nm and 660 nm) and five light intensity levels (35 µE m^{-2} s^{-1} to 104 µE m^{-2} s^{-1}). The flags indicate standard errors.

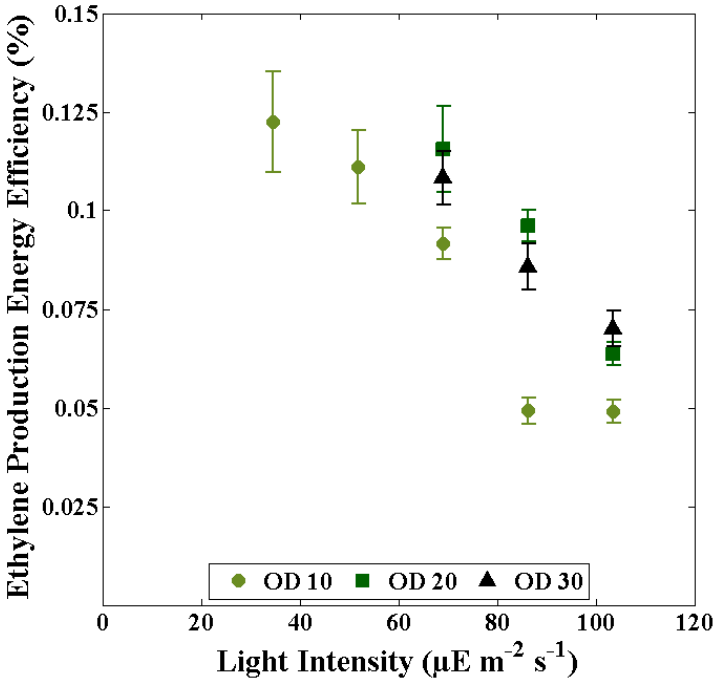

Figure 5.5 Conversion efficiency from light incident on the algal culture to energy contained in ethylene secreted by *Synechocystis* PCC 6803 2x EFE at 630 nm. The figure shows results obtained at three culture densities (OD_{730} of 10, 20 and 30) and five light intensity levels (35 µE m^{-2} s^{-1} to 104 µE m^{-2} s^{-1}). The flags indicate standard errors.

Figure 5.4 and **Figure 5.5** show the PE for the above described experiments in terms of lower heating value of ethylene produced. As with volumetric production rates, there was no significant difference observed in the photosynthetic efficiencies between red (630nm) and deep red (660 nm) illumination sources at all five intensities of the incident light (**Figure 5.4**). Although the production rates peaked at intermediate intensities at both wavelengths, PE monotonically decreased with increasing intensity (p-value < 0.001). This implies that even though a rise in number of incident photons led to more photons being utilized by the algae – thus improving volumetric production rates – they were overall utilized less efficiently. A similar

monotonically decreasing trend with an increase in light intensity was also observed for higher OD cultures (**Figure 5.5**).

Further, PE was found to be dependent on culture density, with the regression model indicating that PE is concave in OD (p-value < 0.01). The initial increase in PE can be attributed to a larger portion of the provided photons being utilized by the greater number of algae in a denser culture. However, on further increase of culture density the light distribution within a stack becomes suboptimal with the algae near the waveguide incapable of utilizing all provided photons and the algae in the interior of the stack being limited due to strong self-shading.

In general, the photosynthetic efficiencies associated with ethylene production were low, with maximum values around 0.125% (**Figure 5.4**). The low efficiencies are primarily due to the current state of genetic modification of the organism, which utilizes the majority of the fixed carbon for biomass production while only a limited portion is channeled towards ethylene synthesis(Ungerer et al., 2012). Consequently only a small fraction of the energy is stored in ethylene molecules. With this consideration, we also calculated PE of biomass production under maximal ethylene production conditions (*i.e.* for OD_{730} 20 at 630 nm and 86 µE m^{-2} s^{-1}). The average change in OD_{730} was measured to be 1.39 units over the course of 2.5 hours (data not shown), leading to a PE of light to biomass conversion of ~15%. This value is two to threefold higher than the PE published for conventional closed PBR(Tredici and Zittelli, 1998). The improvement can be mainly attributed to the use of red light, which minimizes energy losses in photosystems I and II.

5.5 Discussion

5.5.1 Optimization of Short Light-path stacked PBR Varying Wavelength and Intensity

The results described above are aimed at performance optimization of the S-PBR. Two illumination variables, wavelength and intensity of the supplied light, were investigated. The experiments showed that incident light of both red (630 nm) and deep red (670 nm) wavelengths is readily utilized by S. PCC 6803 2x EFE for growth and ethylene production. The obtained results are consistent with earlier studies showing algal growth under red light(Gordon and Polle, 2007; Matthijs et al., 1996; Wang et al., 2007; Zhao et al., 2013). From an overall efficiency point of view, the use of red light is preferable due to lower energy dissipation per photon captured in photosystem I or II. It is estimated that photosynthesis driven by red light is five times more energy efficient than under broad-spectrum solar light(Gordon and Polle, 2007). As no significant differences were found in growth and ethylene production under red and deep red light, the latter should be preferred to improve photosynthetic efficiencies, albeit the achievable difference is only about 5%.

Light energy required per unit volume increases with the density of the culture. In conventional PBRs this is achieved by supplying high light intensities at the reactor surface, with photoinhibition as an unwanted side effect. Due to fast light attenuation along the light path, intensities in the interior of the reactor rapidly become too low to support growth, *i.e.* result in photolimitation(Carvalho et al., 2011; Grima et al., 1996; Johan U Grobbelaar, 2008; Long and Humphries, 1994; Richmond et al., 2003). A high surface-to-volume ratio is therefore desirable to uniformly distribute light across the culture volume. This is realized in the S-PBR by using the stacked waveguide architecture combined with thin light paths. The highest production rate of 937 µg L^{-1} h^{-1} was attained at OD_{730} of 20 and an intensity of 86 µE m^{-2} s^{-1}. This is a nearly two

times improvement over the production rates of 510 µg L^{-1} h^{-1} reported earlier(Jung et al., 2014), and a fourfold improvement over the maximal production rate of 244 µg L^{-1} h^{-1} achieved in a conventional flat-plate PBR (3 cm light path; illuminated from one side at 200 µE m^{-2} s^{-1})(Jung et al., 2014).

Even though the volumetric productivity was concave in nature, as confirmed by the regression model, the production levels around the maximal production rate varied little with a decrease in intensity. This was further borne out by the low coefficient values of the quadratic term, indicative of small differentials around the optimum, in the regression model (See SI). Therefore, economic considerations could dictate operation at a lower intensity in order to achieve higher PE, since the latter decreases with increasing intensity(Carvalho et al., 2011). This would reduce the area required for solar collectors, lowering the capital investment costs.

5.5.2 Demonstration of High Culture Density and Areal Yields

We demonstrated that the carrying capacity of the current S-PBR lies between OD_{730} of 20 and 30, corresponding to CDW of 9 to 14 g L^{-1}. Additionally, due to the stackable design, high areal yields between 115 and 173 g m^{-2} have been achieved. This represents a seven to tenfold improvement in biomass density and a fourfold improvement in areal density compared to the control conventional flat-plate PBR(Jung et al., 2014). High volumetric productivities are advantageous both if algae are used as a biocatalyst secreting biofuel or biofuel precursors (as supported in the S-PBR) or directly as high-energy biomass. The downstream processing of the biomass requires energy intensive dewatering (up to 1 kWh m^{-3} (Molina Grima et al., 2003)), for which the cost per unit product can be reduced by harvesting dense cultures. Thus, production of

high density cultures, such as achievable in S-PBR, will be key determinants for economic viability(Yusuf, 2007).

5.5.3 Integrated System Design

The current S-PBR is an intermediate step in the development of a full-grown technology. In the present work we have first optimized the illumination parameters. A second bottleneck in PBR development is appropriate gas exchange. Sufficient CO_2 needs to be provided as a carbon source for cell growth while O_2 must be removed to avoid toxic concentrations(Carvalho et al., 2006; Greenwell et al., 2010). High gas exchange rates are of particular importance in high density cultures due to the high volumetric reaction rates catalyzed by these cultures. Integration of S-PBR with membrane-based gas transfer, such as achieved through hollow fibers(Carvalho et al., 2006; Ferreira et al., 1998; Greenwell et al., 2010; Kumar et al., 2010), is a promising way to improve productivity by alleviating inhibitions possibly caused by oxygen toxicity and carbon depletion. Hollow fibers would further increase apparent yields by preventing culture displacement due to gas production. Additionally, the present reactor design supports secreted gas products, further necessitating adequate gas exchange to enable extraction of said products. The ability to extract ethylene through hollow fibers has already been successfully tested in preliminary experiments (results not shown).

In conventional systems most mixing energy is required to circulate cells across the light gradient and guarantee adequate gas transfer. The S-PBR as described here, *i.e.* using a combination of slab waveguides and short light path for optimal light delivery, and integrated with hollow fibers for gas exchange, could reduce the amount of mixing required. As mixing contributes 13 to 52% of total construction and operation costs of conventional closed

PBR(Norsker et al., 2011), decrease in mixing requirements is key to make large-scale production of biofuels cost-effective(Wijffels and Barbosa, 2010).

In the long term, the stacked PBR can be integrated with spectral splitting technology. These systems allow selection of narrow bands of solar light, while diverting other wavelengths. In the particular case of the S-PBR, lower energy red photons can be utilized for algal biofuel production while the higher energy blue and green wavelengths are used for other applications, for example generation of electricity through solar photovoltaics(Cuaresma et al., 2009). Additionally, the ultraviolet regime of the light spectrum can be diverted for disinfection of the S-PBR when required. The efficacy of such treatment via etched slab waveguides has also been recently demonstrated(Doud et al., 2014). Further improvements in efficiency can be obtained by using flashing light of frequencies greater than 1 Hz. This approach has been proven to increase photosynthetic rates and energy efficiencies(Johan U. Grobbelaar, 2008; Grobbelaarl et al., 1996). The optical fibers and slab waveguides used in the S-PBR can easily be used to efficiently transfer pulsed light, as is currently done on large scale in optical cables used in communication networks.

The presented work forms a first step in the optimization of the earlier developed stacked photobioreactor with internal illumination through slab waveguides. Optimizing only illumination, fourfold ethylene production rates and up to tenfold higher biomass density accumulation has been shown as compared to a conventional flat-plate PBR. We suggest further improvements, including incorporation of hollow fibers for efficient gas transfer, and integration of the stacked PBR with solar collectors and spectral splitting technology to achieve integrated, holistic systems for future algal biofuel production.

CHAPTER 6

CONCLUSIONS

6.1 Summary

In this dissertation, the focus was to extend the capabilities of the field of optofluidics by development of devices which can penetrate the areas still inaccessible to this versatile tool. To this end, a biocompatible hydrogel waveguide capable of encapsulating live cells within the core of the waveguide to allow interaction of the biology with the strongest optical field in the system, was demonstrated. Integration of microfluidics further extended the capability of the device by bringing into possibility of combining sensing or drug delivery applications (Chapter 3).

New algal photobioreactor architecture was also developed by again utilizing the benefits offered by optofluidics. A benchtop scale stacked waveguide photobioreactor was fabricated and ethylene producing algae was culture within the reactor to verify the validity of the design concept. The growth rates and ethylene production rates measured in the stacked waveguide photobioreactor, clearly demonstrated the benefits afforded by the thin light path architecture (Chapter 4). These capabilities were further extended by optimizing the illumination conditions – wavelength and intensity – and determining the optimal carrying capacity of the photobioreactor. These improvements led to fourfold increase of ethylene production rates as compared to a conventionally run photobioreactor(Chapter 5). Analytical models for determining light and temperature distribution in a full scale system were also created and provided with optimal light and cooling conditions as a culture grows within the reactor (Appendix 1 and 2). A predictive model for UV sterilization of a slab waveguide reactor was also developed – thus comprising another important consideration in a full scale model.

6.2 Future Outlook

The work here described the successful implementation of optofluidics concept to applications in energy and biology. However, the devices fabricated are still restricted to the laboratory and need further development and integration with other technologies to bring the devices out of the laboratory. Even though the agarose hydrogel waveguide described in Chapter 3 were shown to be capable of live cell encapsulation, it would be necessary to move from a standard optical waveguide structure to fabricate more complicated optical elements like Mach Zehnder Interferometers. Moreover, the possibility of using these devices for developing as implantable optical devices should be explored.

Chapter 4 and 5 detailed a new architecture in photobioreactor design which showed substantial improvements over control bioreactors in terms of both growth and ethylene production. However, to scale these photobioreactors to a commercial plant, it might be useful to incorporate technologies like hollow fibre gas membranes for easy extraction of the gaseous products (and oxygen) and deliver carbon-di-oxide directly. A detailed economic analysis would be advisable to identify places in the whole process chain where it would be necessary include innovative strategies to mitigate costs. One such idea could to use the red spectrum, as identified the productive regime in Chapter 5, for photobioreactor functioning while utilizing the rest of spectrum for co-generation of electricity through solar photovoltaics. Alternatively, the capability of the stacked architecture to uniformly distribute light in a scalable manner can be used to develop photocatalysis based applications – for fuel production or solar disinfection of water

APPENDIX

Appendix 1

Calculation and analysis of light distribution inside stacked photobioreactor architecture

As demonstrated in Chapter 4 and Chapter 5, the stacked waveguide photobioreactor (SW-PBR) provides a method to provide optimum distribution of light throughout the volume of the photobioreactor. Therefore, it is therefore important to quantitatively analyze the light distribution in such an architecture especially when it is scaled up. This should enable one to determine the optimal intensity to be coupled into each waveguide for effective utilization by algae.

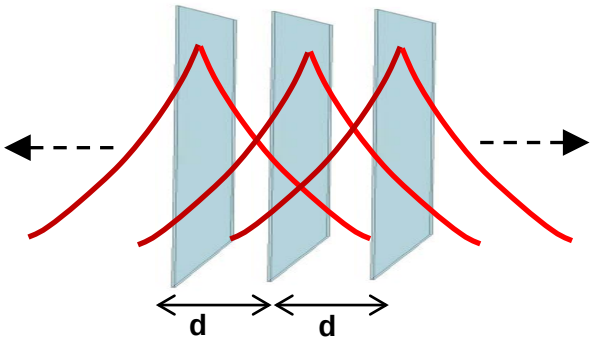

Figure A1.1 Schematic of light distribution in a stacked architecture. Light decays exponentially between each waveguide due to absorbtion but components from other waveguides increase the overall intensity**.**

As seen in **Figure A1.1**, the light distribution within each stack consists of both the exponential decaying light emanating from the two encompassing waveguides, and contributions from all the other waveguides in the stack. The following assumptions are made to calculate the light distribution:

a) Absorbtion by the algae between the slides follows Beer Lambert's Law :

$$I(x) = I_0 \exp(-\alpha x) \qquad \textbf{(A1.1)}$$

b) Absorbtion Coefficient α is estimated through Optical Density (OD) of the algae solution :

$$OD = -\log_{10}(I_t / I_0) \qquad \textbf{(A1.2)}$$

Where, I_0 is the light intensity emanating from the surface of the waveguide

I_t is the transmitted intensity after 1 cm through the culture solution

Based on this, the general solution for a finite stack, where x=0 indicates the centre of the stack, is as follows:

For 2L+1 waveguides, the light intensity between x= k*d and (k+1)*d is given by:

$$I(x) = I_0\{e^{-\propto(x-kd)}\ (1-e^{-\propto(L+k+1)d}) + e^{\propto(x-(k+1)d)}(1 - e^{-\propto(L-k)d})\}/\{1-(e^{-\propto d})\} \quad \text{(A1.3)}$$

This can be generalized to an infinite stack with the following expression:

$$I(x) = I[e^{-\propto(x)} + e^{\propto(x-d)}]/\{1-(e^{-\propto d})\} \quad \text{(A1.4)}$$

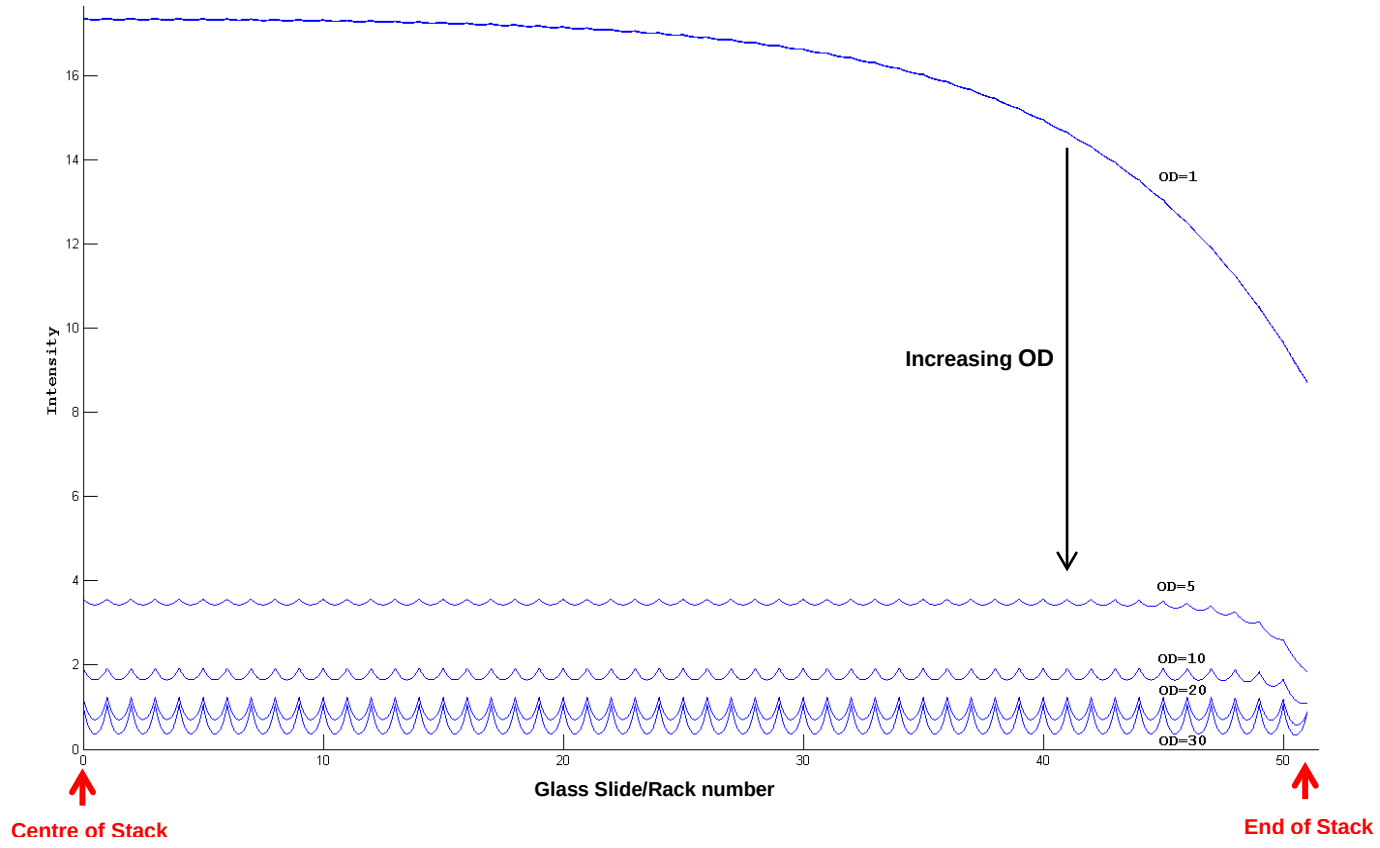

Figure A1.2 Theoretical light distribution within a stacked photobioreactor as a function of OD. The intensity within the stack decreases as OD increases due to increased absorbtion. Only half the stack is represented (the other half is symmetric) and it is assumed that one unit of light energy is emanating from each waveguide.

The calculated light distribution is shown in **Figure A1.2.** As can be seen, the light intensity within the stack decreases as the OD of the culture within the stack increases (assuming same light intensity) due to

higher absorbtion. Also, to be noted is the fact that as the OD increases, the light intensity across the stacks becomes more uniform, even at the end of the photobioreactor, since contribution from other waveguides becomes minimal. However, the light intensity with each stack shows a significant attenuation due to high absorbtion. This can be used to calculate the carrying capacity of the stacked photobioreactor based on the optimum levels of light for the particular algal species. Alternatively, as shown in Figure A1.3, it can also be used to calculate the optimum light intensity required for a particular optical density of the culture. This is particularly useful since this can be used to modify and optimize the light intensity coupled into each waveguide as the culture grows (and hence, increases its OD).

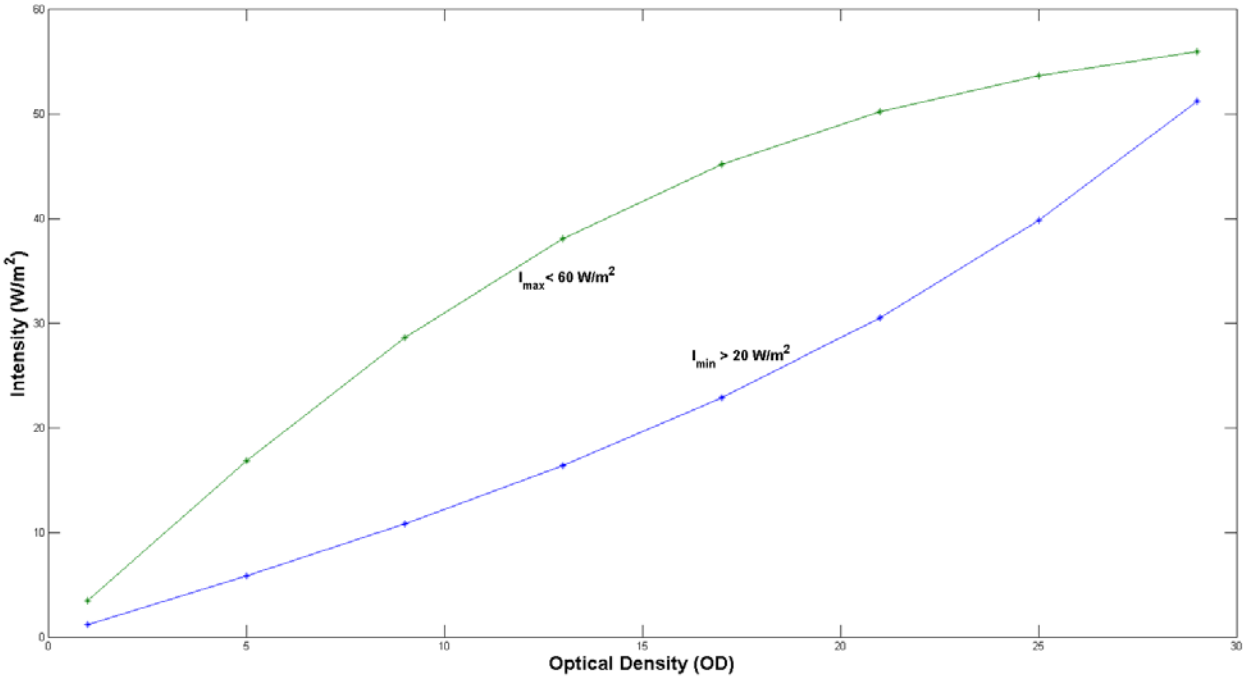

Figure A1.3 Optimal light intensity envelope as a function of optical density of the culture. It is assumed that the minimum and maximum optimal intensities are 20 W m^{-2} and 60 W m^{-2} respectively. The envelope could be scaled according to the necessary intensities using the equations derived above.

The calculations shown here hence provide a method to determine the light distribution within a stacked architecture and hence, calculate determine the optimal light intensity within each waveguide to be coupled as the culture grows within the photobioreactor.

Appendix 2

Analysis of thermal profiles in a stacked waveguide photobioreactor (SW-PBR)

Non photochemical quenching (NPQ) is a photosynthetic process in which excess light absorbed by the photosynthetic centers is removed as heat to protect the cellular mechanism. This could lead to a substantial temperature rise in the SW-PBR due to the high culture densities possible in the photobioreactor, and subsequently high absorbtion in the stacked photobioreactor, and low exposed surface area to dissipate the generated heat. Algae and their production are known to be sensitive to temperature, with production dropping drastically at higher temperatures. This therefore necessitates an analysis of temperature profiles based on the light distribution calculated previously for a possible full scale system.

Two possible full scale designs were chosen for analysis to that end and are shown in **Figure A2.1 and A2.2.**

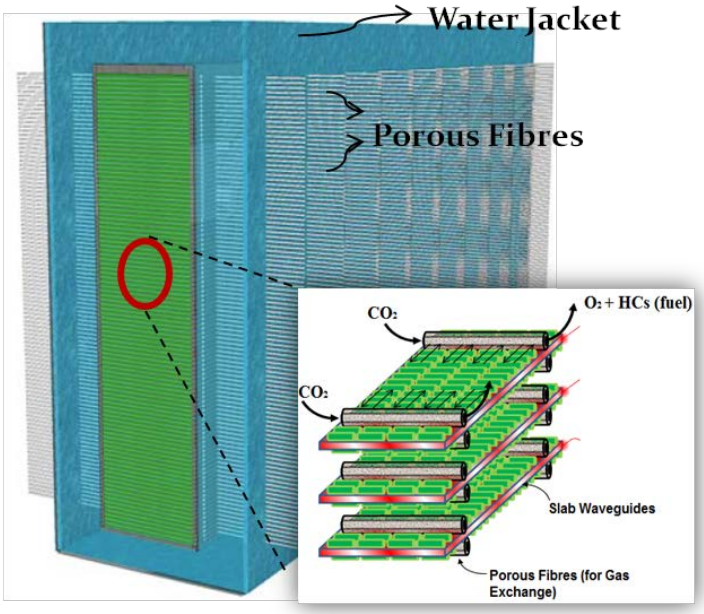

Figure A2.1 Single stack photobioreactor design with a water jacket for cooling. The single stack design provides improved volume efficiency but leads to increased heat entrapment due to lower exposed area for heat dissipation.

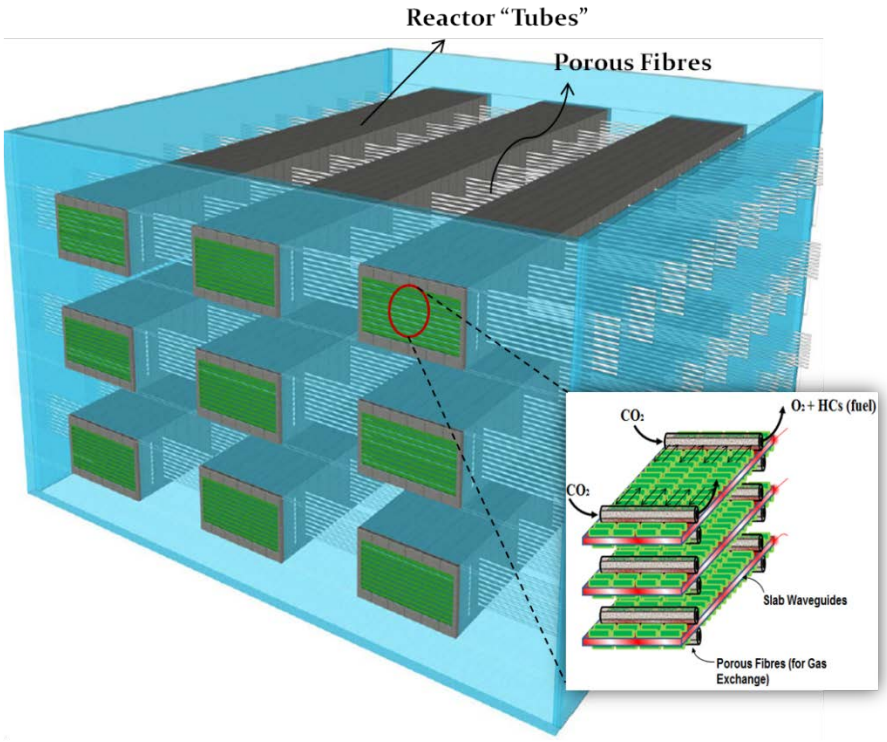

Figure A2.2 Distributed "tubular" stack photobioreactor design. The distributed stack design leads to decreased volume efficiency but improves heat dissipation due to higher surface area of the tubes.

A simulation model was created in finite element solver COMSOL to analyze the heat profiles within the two designs depicted. The following assumptions were input into the model to provide an upper bound to the temperature rise in the photobioreactors:

1) All light incident on the photobioreactor is converted to heat due to NPQ. This assumption can be improved by performing experiments on the algae to more accurately determine the degree of NPQ in the organism
2) The walls were assumed to be fabricated of a polymeric material specifically PDMS, while the waveguides were assumed to be fabricated from glass.
3) For the single stack design (**Figure A2.1**), simulations were carried out on a single stack model with periodic boundary conditions on the top and bottom surfaces to simulate the center of a large single stack, since this is where the maximum temperature rise is to be expected.

4) Free convective boundary conditions are applied at the outer surfaces of the photobioreactors with options of both air-cooling (heat transfer coefficient = 8 W/m^2K) and water cooling (heat transfer coefficient = 2300 W/m^2K) simulated to yield optimal conditions.

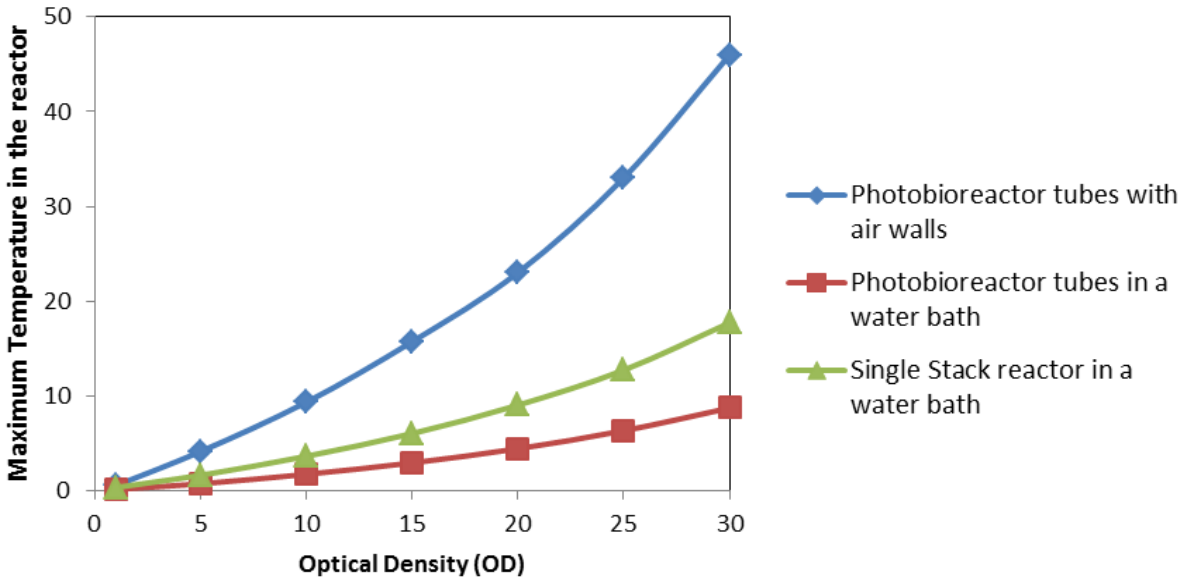

Figure A2.3 Maximum temperature rise within the photobioreactor as a function of OD for different photobioreactor designs and convective cooling. The light intensity used for the calculation is as derived earlier.

Figure A2.3 shows the maximum temperature rise in the two photobioreactor designs with both air-cooled and water-cooled convection boundaries. The temperature rise is seen as a function of OD to again analyze the temperature in the photobioreactor as the culture grows within. The light intensity for the simulations are obtained from the calculations shown in Appendix 1. The results indicate that high culture densities it might be necessary to cool both photobioreactor designs with a water jacket as free air convection would not be enough to sustain optimal temperatures within the photobioreactor.

Appendix 3

Supplementary Information for Chapter 5: Results of the regression analysis

Two regression models were fitted to the data, one for ethylene production rates (Table 1) and one for photosynthetic efficiency of ethylene production (Table 2). In both cases the wavelength and intensity of the incident light and the culture OD were used as explanatory variables. In both models the regression coefficient associated with wavelength was found not to be statistically significant (p-value > 0.9) and was hence subsequently removed from the regression model. Additionally, removing wavelength as an explanatory variable did not reduce the R^2-value, further justifying its removal. However, despite a non-significant coefficient (p-value = 0.166), the interaction term between OD and intensity, in the model for ethylene production rates was retained. This was as both theoretical considerations (*i.e.* optimal intensity is expected to increase with increasing OD) and a reduction in the R^2-value supported the inclusion of the interaction term. On the other hand, for regression analysis for PE, the interaction term (p-value > 0.85) was not included in the final model since there was neither a strong theoretical reason to support its existence, nor did it lead to an improvement of the R^2-value.

Table A4.1. Regression coefficients for model of the dependence of ethylene production rates on intensity, wavelength and OD.

	Estimate	**Std. Error**	**Pr(>|t|)**	
Intercept	-462.80529	151.39989	0.00307	
OD²	-1.41317	0.31497	2.49e-05	***
Intensity²	-0.14366	0.03009	8.40e-06	***
OD	55.22942	15.42941	0.00060	**
Intensity	18.72381	3.80967	4.90e-06	***
OD:Intensity	0.15401	0.11014	0.16604	

Signif. codes: 0 '***' 0.001 '**' 0.01 '*' 0.05 '.' 0.1 ' ' 1

Residual standard error: 112.2 on 76 degrees of freedom

Multiple R-squared: 0.6432, Adjusted R-squared: 0.6151

F-statistic: 22.84 on 6 and 76 DF, p-value: 3.244e-15

Table A4.2. Regression coefficients for model of the dependence of photosynthetic efficiency of ethylene production on intensity, wavelength and OD.

	Estimate	**Std. Error**	**Pr(>|t|)**	**Significance**
Intercept	1.140e-03	1.291e-04	2.05e-13	***
OD	6.900e-05	1.637e-05	6.61e-05	***
OD^2	-1.436e-06	4.158e-07	0.000889	**
Intensity	-1.197e-05	7.807e-07	< 2e-16	***

Significance codes (for FWER of 0.05): 0 '***' 0.001 '**' 0.01 '*' 0.05 '.' 0.1 ' ' 1

Residual standard error: 0.0001474 on 79 degrees of freedom

Multiple R-squared: 0.7487, Adjusted R-squared: 0.7391

F-statistic: 78.44 on 3 and 79 DF, p-value: < 2.2e-16

Appendix 4

Predictive model for *in-situ* UV disinfection of a slab-waveguide photobioreactor

Adapted partially from: "*In-situ* UV disinfection of a slab-waveguide photobioreactor", Devin F. R. Doud, Aadhar Jain, Syed S. Ahsan, David Erickson, and Largus T. Angenent. Submitted to Environmental Science and Technology (2014).

Contamination of a photobioreactor is a major problem which can lead to substantial costs associated with disinfecting the photobioreactor. To counter this in a waveguide based photobioreactor like ours, we investigated a method to *in-situ* disinfect the bioreactor by UV sterilization. This can be accomplished by using the waveguides to transmit UV light to the culture instead of the visible wavelengths. We developed a model to determine the degree of disinfection in a single waveguide reactor as a function of operational parameters – intensity, time of treatment, disinfection constant of the contaminant and the depth of the reactor.

The Chick-Watson model for disinfection serves as the foundation for the model and is represented in equation A4.1.

$$N = N_O \exp(-kt) \qquad \text{(A4.1)}$$

Where, N represents the number of contaminants remaining after treatment

N_o represents the initial number of contaminants

t represents the treatment time

k represents the disinfection rate constant specific to the organism *i.e.* the dosage required per unit time for 1 log reduction

This can be converted to a UV specific form by incorporating the total UV dosage incident at a particular depth in the chamber represented as TD(x,t) in equation A4.2 below.

$$\frac{N}{N_O}(x,t) = \exp(-TD(x,t)K_O) \qquad \text{(A4.2)}$$

$$TD\ (x,t) = I_O t \exp(-\alpha x) \qquad \text{(A4.3)}$$

$$\alpha = -100 \cdot \ln 10^{-OD_{254}} \qquad \text{(A4.4)}$$

$$Corrected\ TD(x,t) = I_O t \exp(-\alpha f x) \qquad \text{(A4.5)}$$

where α represents the absorbtion coefficient of the culture solution and is therefore a function of the optical density (OD_{254}) at the sterilization wavelength (254 nm), K_o is a measure of disinfection achieved at a dosage level and x represents the distance into the reactor chamber away from the waveguide surface.

A correction factor 'f' is introduced in the expression for total dosage (equation A4.5) to correct for the 3-dimensional scattering from the waveguide (due to random pitting of the surface) rather than the 2-dimensional assumed for the model. The factor 'f' is greater than 1 since the ray has to travel a distance larger than the 2-dimensional depth, and therefore leads to greater absorbtion.

Substituting equation A4.5 in A4.2 and integrating over the volume of the reactor leads to the following expression for proportion of cells remaining in the volume after treatment.

$$\frac{1}{\alpha f d}\left[E_i\left(k \cdot \exp\left(-\alpha f d\right)\right) - E_i\left(k\right)\right] \qquad \text{(A4.6)}$$

$$k = K_o I_o t \qquad \text{(A4.7)}$$

where d is the depth of the channel, E_i represents the exponential integral function.

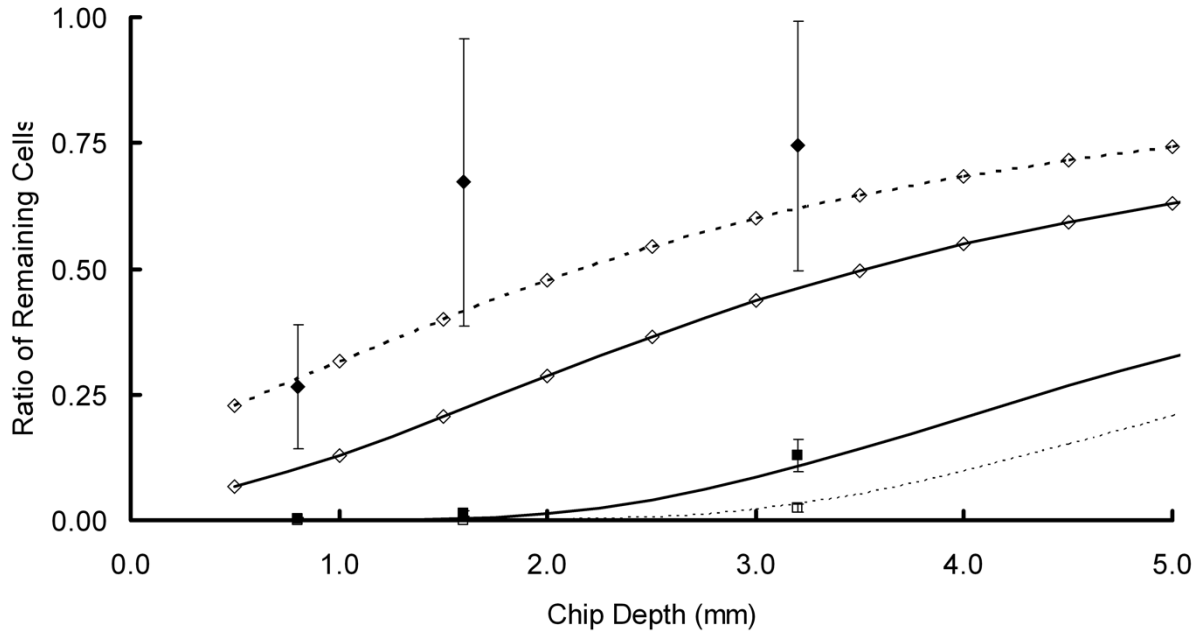

Figure A4.1 Model prediction for *B. subtilis* spore disinfection compared to empirical results. The model was fitted to six *E. coli* data points for chemical etch bioreactors for 75 and 150-min exposures. Solid and open squares indicate 75- and 150-min exposures, respectively, with the standard deviations shown. Solid and dotted lines correspond to predicted disinfection for 75 and 150-min exposures with k values of 17.5 and 35, respectively, with a fitted f value of 2.6. *B. subtilis* spore data is represented by filled diamonds with the standard deviations shown. The function predicted by our model with k value 3.5 is represented by a solid line with open diamonds, while the k value of 1.9 is represented by dotted line with open diamonds.

The model was verified experimentally (experiments conducted by Devin Doud) by determining the parameters f and k by fitting the theoretical curve to the experimental data obtained for E.coli. These values were modified for *B. subtilis* spore by changing the value of k according to the values in the literature and the treatment time. As can be seen from **Figure A4.1,** the theoretical curve fit the experimental data within experimental error thus verifying the validity of the model.

BIBLIOGRAPHY

1. Ashkin, A., Dziedzic, J.M., 1987. Optical trapping and manipulation of viruses and bacteria. Science 235, 1517–1520. doi:10.1126/science.3547653
2. Cao, Z., Gilbert, R.J., He, W., 2009. Simple Agarose- Chitosan Gel Composite System for Enhanced Neuronal Growth in Three Dimensions. Biomacromolecules 10, 2954–2959.
3. Cheng, S.-Y., Heilman, S., Wasserman, M., Archer, S., Shuler, M.L., Wu, M., 2007. A hydrogel-based microfluidic device for the studies of directed cell migration. Lab Chip 7, 763–769. doi:10.1039/b618463d
4. Dancil, K.S., Greiner, D.P., Sailor, M.J., 1999. A porous silicon optical biosensor: Detection of reversible binding of IgG to a protein A-modified surface. J. Am. Chem. Soc. 121, 7925–7930. doi:10.1021/ja991421n
5. Ding, L., Blackwell, R.I., Künzler, J.F., Knox, W.H., 2008. Femtosecond laser micromachining of waveguides in silicone-based hydrogel polymers. Appl. Opt. 47, 3100–3108. doi:10.1364/AO.47.003100
6. F??rster, T., Strohh??fer, C., Bock, K., Kasak, P., Danko, M., Kronekova, Z., Nedelcev, T., Krupa, I., Lacik, I., 2009. Biosensor for calcium based on a hydrogel optical waveguide with integrated sensor proteins, in: TRANSDUCERS 2009 - 15th International Conference on Solid-State Sensors, Actuators and Microsystems. pp. 1218–1221. doi:10.1109/SENSOR.2009.5285877
7. Fan, X., White, I.M., Shopova, S.I., Zhu, H., Suter, J.D., Sun, Y., 2008. Sensitive optical biosensors for unlabeled targets: A review. Anal. Chim. Acta. doi:10.1016/j.aca.2008.05.022
8. Homola, J., Yee, S.S., Gauglitz, G., 1999. Surface plasmon resonance sensors: review. Sensors Actuators, B Chem. 54, 3–15. doi:10.1016/S0925-4005(98)00321-9
9. Koo, J.S., Smith, P.G.R., Williams, R.B., Riziotis, C., Grossel, M.C., 2003. UV written waveguides using crosslinkable PMMA-based copolymers. Opt. Mater. (Amst). 23, 583–592. doi:10.1016/S0925-3467(03)00025-9
10. Ling, Y., Rubin, J., Deng, Y., Huang, C., Demirci, U., Karp, J.M., Khademhosseini, A., 2007. A cell-laden microfluidic hydrogel. Lab Chip 7, 756–762. doi:10.1039/b615486g
11. Moskaluk, C.A., Stoler, M.H., 2002. Agarose mold embedding of cultured cells for tissue microarrays. Diagn. Mol. Pathol. 11, 234–238. doi:10.1097/00019606-200212000-00007

12. Park, T.G., 1999. Temperature modulated protein release from pH/temperature-sensitive hydrogels. Biomaterials 20, 517–521. doi:10.1016/S0142-9612(98)00197-5
13. Richter, A., Paschew, G., Klatt, S., Lienig, J., Arndt, K.-F., Adler, H.-J.P., 2008. Review on Hydrogel-based pH Sensors and Microsensors. Sensors. doi:10.3390/s8010561
14. Sakai, S., Hashimoto, I., Kawakami, K., 2007. Synthesis of an agarose-gelatin conjugate for use as a tissue engineering scaffold. J. Biosci. Bioeng. 103, 22–6. doi:10.1263/jbb.103.22
15. Sowa, S., Watanabe, W., Tamaki, T., Nishii, J., Itoh, K., 2006. Symmetric waveguides in poly(methyl methacrylate) fabricated by femtosecond laser pulses. Opt. Express 14, 291–297. doi:10.1364/OPEX.14.000291
16. Stevens, M.M., Mayer, M., Anderson, D.G., Weibel, D.B., Whitesides, G.M., Langer, R., 2005. Direct patterning of mammalian cells onto porous tissue engineering substrates using agarose stamps. Biomaterials 26, 7636–7641. doi:10.1016/j.biomaterials.2005.05.001
17. Suzuki, A., Tanaka, T., 1990. Phase transition in polymer gels induced by visible light. Nature 346, 345–347.
18. Tanaka, T., 1978. Collapse of Gels and the Critical Endpoint. Phys. Rev. Lett. 40, 820–823. doi:10.1103/PhysRevLett.40.820
19. Wang, Y., Huang, C.-J., Jonas, U., Wei, T., Dostalek, J., Knoll, W., 2010. Biosensor based on hydrogel optical waveguide spectroscopy. Biosens. Bioelectron. 25, 1663–1668. doi:http://dx.doi.org/10.1016/j.bios.2009.12.003
20. Yang, A.H.J., Moore, S.D., Schmidt, B.S., Klug, M., Lipson, M., Erickson, D., 2009. Optical manipulation of nanoparticles and biomolecules in sub-wavelength slot waveguides. Nature 457, 71–75. doi:10.1038/nature07593
21. An, J.Y., Kim, B.W. 2000. Biological desulfurization in an optical-fiber photobioreactor using an automatic sunlight collection system. *Journal of Biotechnology*, **80**(1), 35-44.
22. Beal, C.M., Hebner, R.E., Webber, M.E., Ruoff, R.S., Seibert, A.F. 2012a. The Energy Return on Investment for Algal Biocrude: Results for a Research Production Facility. *Bioenergy Research*, **5**(2), 341-362.

23. Beal, C.M., Stillwell, A.S., King, C.W., Cohen, S.M., Berberoglu, H., Bhattarai, R.P., Connelly, R.L., Webber, M.E., Hebner, R.E. 2012b. Energy return on investment for algal biofuel production coupled with wastewater treatment. *Water Environ Res*, **84**(9), 692-710.
24. Brennan, L., Owende, P. 2010. Biofuels from microalgae—A review of technologies for production, processing, and extractions of biofuels and co-products. *Renewable and Sustainable Energy Reviews*, **14**(2), 557-577.
25. Chen, C.-Y., Yeh, K.-L., Aisyah, R., Lee, D.-J., Chang, J.-S. 2011. Cultivation, photobioreactor design and harvesting of microalgae for biodiesel production: A critical review. *Bioresource Technology*, **102**(1), 71-81.
26. Chen, C.Y., Lee, C.M., Chang, J.S. 2006. Hydrogen production by indigenous photosynthetic bacterium Rhodopseudomonas palustris WP3-5 using optical fiber-illuminating photobioreactors. *Biochemical Engineering Journal*, **32**(1), 33-42.
27. Chisti, Y. 2007. Biodiesel from microalgae. *Biotechnol Adv*, **25**(3), 294-306.
28. Chisti, Y. 2008. Biodiesel from microalgae beats bioethanol. *Trends in Biotechnology*, **26**(3), 126-131.
29. Chisti, Y., Yan, J. 2011. Energy from algae: Current status and future trends: Algal biofuels – A status report. *Applied Energy*, **88**(10), 3277-3279.
30. Choi, H.J., Lee, J.M., Lee, S.M. 2013. A novel optical panel photobioreactor for cultivation of microalgae. *Water Science and Technology*, **67**(11), 2543-2548.
31. Corbett, L.L., Parker, D.L. 1976. Viability of Lyophilized Cyanobacteria (Blue-Green-Algae). *Applied and Environmental Microbiology*, **32**(6), 777-780.
32. Dye, D., Muhs, J., Wood, B., Sims, R. 2011. Design and Performance of a Solar Photobioreactor Utilizing Spatial Light Dilution. *Journal of Solar Energy Engineering-Transactions of the Asme*, **133**(1).
33. Janssen, M., de Bresser, L., Baijens, T., Tramper, J., Mur, L., Snel, J.H., Wijffels, R. 2000. Scale-up aspects of photobioreactors: effects of mixing-induced light/dark cycles. *Journal of Applied Phycology*, **12**(3-5), 225-237.
34. Janssen, M., Tramper, J., Mur, L.R., Wijffels, R.H. 2003. Enclosed outdoor photobioreactors: Light regime, photosynthetic efficiency, scale-up, and future prospects. *Biotechnology and Bioengineering*, **81**(2), 193-210.

35. Jung, E.E., Kalontarov, M., Doud, D.F., Ooms, M.D., Angenent, L.T., Sinton, D., Erickson, D. 2012. Slab waveguide photobioreactors for microalgae based biofuel production. *Lab Chip*, **12**(19), 3740-5.

36. Kalontarov, M., Doud, D.F.R., Jung, E.E., Angenent, L.T., Erickson, D. 2013. In situ hollow fiber membrane facilitated CO2 delivery to a cyanobacterium for enhanced productivity. *RSC Advances*, **3**(32), 13203-13209.

37. Lee, C.G., Palsson, B.O. 1994. High-Density Algal Photobioreactors Using Light-Emitting-Diodes. *Biotechnology and Bioengineering*, **44**(10), 1161-1167.

38. Lehr, F., Posten, C. 2009. Closed photo-bioreactors as tools for biofuel production. *Curr Opin Biotechnol*, **20**(3), 280-5.

39. Mata, T.M., Martins, A.A., Caetano, N.S. 2010. Microalgae for biodiesel production and other applications: A review. *Renewable and Sustainable Energy Reviews*, **14**(1), 217-232.

40. Molina Grima, E., Fernández, F.G.A., García Camacho, F., Chisti, Y. 1999. Photobioreactors: light regime, mass transfer, and scaleup. *Journal of Biotechnology*, **70**(1–3), 231-247.

41. Ooms, M.D., Sieben, V.J., Pierobon, S.C., Jung, E.E., Kalontarov, M., Erickson, D., Sinton, D. 2012. Evanescent photosynthesis: exciting cyanobacteria in a surface-confined light field. *Phys Chem Chem Phys*, **14**(14), 4817-23.

42. Rodolfi, L., Zittelli, G.C., Bassi, N., Padovani, G., Biondi, N., Bonini, G., Tredici, M.R. 2009. Microalgae for Oil: Strain Selection, Induction of Lipid Synthesis and Outdoor Mass Cultivation in a Low-Cost Photobioreactor. *Biotechnology and Bioengineering*, **102**(1), 100-112.

43. Rubio, F.C., Camacho, F.G., Sevilla, J.M., Chisti, Y., Grima, E.M. 2003. A mechanistic model of photosynthesis in microalgae. *Biotechnol Bioeng*, **81**(4), 459-73.

44. Sharma, N.K., Tiwari, S.P., Tripathi, K., Rai, A.K. 2011. Sustainability and cyanobacteria (blue-green algae): facts and challenges. *Journal of Applied Phycology*, **23**(6), 1059-1081.

45. Steffensen, D., Burch, M., Nicholson, B., Drikas, M., Baker, P. 1999. Management of toxic Blue-Green algae (cyanobacteria) in Australia. *Environmental Toxicology*, **14**(1), 183-195.

46. Stephens, E., Ross, I.L., Mussgnug, J.H., Wagner, L.D., Borowitzka, M.A., Posten, C., Kruse, O., Hankamer, B. 2010. Future prospects of microalgal biofuel production systems. *Trends Plant Sci*, **15**(10), 554-64.

47. Torkamani, S., Wani, S.N., Tang, Y.J., Sureshkumar, R. 2010. Plasmon-enhanced microalgal growth in miniphotobioreactors. *Applied Physics Letters*, **97**(4).

48. Ungerer, J., Tao, L., Davis, M., Ghirardi, M., Maness, P.-C., Yu, J. 2012. Sustained photosynthetic conversion of CO2 to ethylene in recombinant cyanobacterium Synechocystis 6803. *Energy & Environmental Science*, **5**(10), 8998-9006.

49. Xue, S.Z., Zhang, Q.H., Wu, X., Yan, C.H., Cong, W. 2013. A novel photobioreactor structure using optical fibers as inner light source to fulfill flashing light effects of microalgae. *Bioresource Technology*, **138**, 141-147.

50. Zittelli, G.C., Biondi, N., Rodolfi, L., Tredici, M.R. 2013. Photobioreactors for Mass Production of Microalgae. in: *Handbook of Microalgal Culture*, John Wiley & Sons, Ltd, pp. 225-266.

51. Aci??n Fern??ndez, F.G., Garc??a Camacho, F., Chisti, Y., 1999. Photobioreactors: light regime, mass transfer, and scaleup. Prog. Ind. Microbiol. 35, 231–247. doi:10.1016/S0079-6352(99)80118-0

52. Beal, C.M., Stillwell, A.S., King, C.W., Cohen, S.M., Berberoglu, H., Bhattarai, R.P., Connelly, R.L., Webber, M.E., Hebner, R.E., 2012. Energy Return on Investment for Algal Biofuel Production Coupled with Wastewater Treatment. Water Environ. Res. 84, 692–710. doi:10.2175/106143012X13378023685718

53. Brennan, L., Owende, P., 2010. Biofuels from microalgae-A review of technologies for production, processing, and extractions of biofuels and co-products. Renew. Sustain. Energy Rev. doi:10.1016/j.rser.2009.10.009

54. Carvalho, A.P., Meireles, L. a, Malcata, F.X., 2006. Microalgal reactors: a review of enclosed system designs and performances. Biotechnol. Prog. 22, 1490–506. doi:10.1021/bp060065r

55. Carvalho, A.P., Silva, S.O., Baptista, J.M., Malcata, F.X., 2011. Light requirements in microalgal photobioreactors: an overview of biophotonic aspects. Appl. Microbiol. Biotechnol. 89, 1275–88. doi:10.1007/s00253-010-3047-8

56. Cheirsilp, B., Torpee, S., 2012. Enhanced growth and lipid production of microalgae under mixotrophic culture condition: effect of light intensity, glucose concentration and fed-batch cultivation. Bioresour. Technol. 110, 510–6. doi:10.1016/j.biortech.2012.01.125

57. Chen, C.-Y., Yeh, K.-L., Aisyah, R., Lee, D.-J., Chang, J.-S., 2011. Cultivation, photobioreactor design and harvesting of microalgae for biodiesel production: a critical review. Bioresour. Technol. 102, 71–81. doi:10.1016/j.biortech.2010.06.159

58. Cuaresma, M., Janssen, M., Vílchez, C., Wijffels, R.H., 2009. Productivity of Chlorella sorokiniana in a short light-path (SLP) panel photobioreactor under high irradiance. Biotechnol. Bioeng. 104, 352–9. doi:10.1002/bit.22394

59. Doud, D.F.R., Jain, A., Ahsan, S.S., Erickson, D., Angenent, L.T., 2014. In-situ UV disinfection of a slab-waveguide photobioreactor.

60. Fan, L.-H., Zhang, Y.-T., Zhang, L., Chen, H.-L., 2008. Evaluation of a membrane-sparged helical tubular photobioreactor for carbon dioxide biofixation by Chlorella vulgaris. J. Memb. Sci. 325, 336–345. doi:10.1016/j.memsci.2008.07.044

61. Ferreira, B.S., Fernandes, H.L., Reis, A., Mateus, M., 1998. Microporous Hollow Fibres for Carbon Dioxide Absorption : Mass Transfer Model Fitting and the Suppl y ing of Carbon Dioxide to Microalgal Cultures.

62. Gordon, J.M., Polle, J.E.W., 2007. Ultrahigh bioproductivity from algae. Appl. Microbiol. Biotechnol. 76, 969–75. doi:10.1007/s00253-007-1102-x

63. Greenwell, H.C., Laurens, L.M.L., Shields, R.J., Lovitt, R.W., Flynn, K.J., 2010. Placing microalgae on the biofuels priority list: a review of the technological challenges. J. R. Soc. Interface 7, 703–26. doi:10.1098/rsif.2009.0322

64. Grima, E.M., Femtidez Sevilla, J.M., Sánchez Pérez, J.A., García Camacho, F., 1996. A study on simultaneous photolimitation and photoinhibition in dense microalgal cultures taking into account incident and averaged irradiances. J. Biotechnol. 45, 59–69.

65. Grobbelaar, J.U., 2008. Factors governing algal growth in photobioreactors: the “open” versus “closed” debate. J. Appl. Phycol. 21, 489–492. doi:10.1007/s10811-008-9365-x

66. Grobbelaar, J.U., 2008. Upper limits of photosynthetic productivity and problems of scaling. J. Appl. Phycol. 21, 519–522. doi:10.1007/s10811-008-9372-y

67. Grobbelaar, J.U., 2010. Microalgal biomass production: challenges and realities. Photosynth. Res. 106, 135–44. doi:10.1007/s11120-010-9573-5

68. Grobbelaarl, J.U., Nedbal, L., Tichy, V., 1996. Influence of high frequency light / dark fluctuations on photosynthetic characteristics of microalgae photoacclimated to different light intensities and implications for mass algal cultivation 335–343.

69. Janssen, M., Tramper, J., Mur, L.R., Wijffels, R.H., 2003. Enclosed outdoor photobioreactors: light regime, photosynthetic efficiency, scale-up, and future prospects. Biotechnol. Bioeng. 81, 193–210. doi:10.1002/bit.10468

70. Jegan, S., Jegathese, P., Farid, M., 2014. Microalgae as a Renewable Source of Energy : A Niche Opportunity 2014.

71. Jung, E.E., Jain, A., Voulis, N., Doud, D.F.R., Angenent, L.T., Erickson, D., 2014. Stacked optical waveguide photobioreactor for high density algal cultures.

72. Katsuda, T., Lababpour, A., Shimahara, K., Katoh, S., 2004. Astaxanthin production by Haematococcus pluvialis under illumination with LEDs. Enzyme Microb. Technol. 35, 81–86. doi:10.1016/j.enzmictec.2004.03.016

73. Kleinegris, D.M.M., Janssen, M., Brandenburg, W. a, Wijffels, R.H., 2011. Two-phase systems: potential for in situ extraction of microalgal products. Biotechnol. Adv. 29, 502–7. doi:10.1016/j.biotechadv.2011.05.018

74. Ku, H.H., 1966. Notes on the Use of Propagation of Error Formulas. J. Res. Natl. Bur. Stand. (1934). 70C, 263–273.

75. Kumar, A., Yuan, X., Sahu, A.K., Dewulf, J., Ergas, S.J., Van Langenhove, H., 2010. A hollow fiber membrane photo-bioreactor for CO2 sequestration from combustion gas coupled with wastewater treatment: a process engineering approach. J. Chem. Technol. Biotechnol. 85, 387–394. doi:10.1002/jctb.2332

76. Kunjapur, A.M., Eldridge, R.B., 2010. Photobioreactor Design for Commercial Biofuel Production from Microalgae. Ind. Eng. Chem. Res. 49, 3516–3526. doi:10.1021/ie901459u

77. Li, Y., Zhou, W., Hu, B., Min, M., Chen, P., Ruan, R.R., 2012. Effect of light intensity on algal biomass accumulation and biodiesel production for mixotrophic strains Chlorella kessleri and Chlorella protothecoide cultivated in highly concentrated municipal wastewater. Biotechnol. Bioeng. 109, 2222–9. doi:10.1002/bit.24491

78. Long, S.P., Humphries, S., 1994. Photoinhibition of Photosynthesis in Nature. Annu. Rev. Plant Mol. Biol. 45, 633–662.

79. Mata, T.M., Martins, A. a., Caetano, N.S., 2010. Microalgae for biodiesel production and other applications: A review. Renew. Sustain. Energy Rev. 14, 217–232. doi:10.1016/j.rser.2009.07.020

80. Matthijs, H.C., Balke, H., van Hes, U.M., Kroon, B.M., Mur, L.R., Binot, R. a, 1996. Application of light-emitting diodes in bioreactors: flashing light effects and energy economy in algal culture (Chlorella pyrenoidosa). Biotechnol. Bioeng. 50, 98–107. doi:10.1002/(SICI)1097-0290(19960405)50:1<98::AID-BIT11>3.0.CO;2-3

81. Molina Grima, E., Belarbi, E.-H., Acién Fernández, F.G., Robles Medina, a, Chisti, Y., 2003. Recovery of microalgal biomass and metabolites: process options and economics. Biotechnol. Adv. 20, 491–515.

82. Norsker, N.-H., Barbosa, M.J., Vermuë, M.H., Wijffels, R.H., 2011. Microalgal production--a close look at the economics. Biotechnol. Adv. 29, 24–7. doi:10.1016/j.biotechadv.2010.08.005

83. Ogbonna, J.C., Soejima, T., Tanaka, H., 1999. An integrated solar and artificial light system for internal illumination of photobioreactors. J. Biotechnol. 70, 289–97.

84. Pires, J.C.M., Alvim-Ferraz, M.C.M., Martins, F.G., Simões, M., 2012. Carbon dioxide capture from flue gases using microalgae: Engineering aspects and biorefinery concept. Renew. Sustain. Energy Rev. 16, 3043–3053. doi:10.1016/j.rser.2012.02.055

85. Posten, C., Schaub, G., 2009. Microalgae and terrestrial biomass as source for fuels--a process view. J. Biotechnol. 142, 64–9. doi:10.1016/j.jbiotec.2009.03.015

86. R Core Team, 2014. R: A language and environment for statistical computing.

87. Richmond, A., Cheng-Wu, Z., Zarmi, Y., 2003. Efficient use of strong light for high photosynthetic productivity: interrelationships between the optical path, the optimal population density and cell-growth inhibition. Biomol. Eng. 20, 229–236. doi:10.1016/S1389-0344(03)00060-1

88. Rodolfi, L., Chini Zittelli, G., Bassi, N., Padovani, G., Biondi, N., Bonini, G., Tredici, M.R., 2009. Microalgae for oil: strain selection, induction of lipid synthesis and outdoor mass cultivation in a low-cost photobioreactor. Biotechnol. Bioeng. 102, 100–12. doi:10.1002/bit.22033

89. Ruangsomboon, S., 2012. Effect of light, nutrient, cultivation time and salinity on lipid production of newly isolated strain of the green microalga, Botryococcus braunii KMITL 2. Bioresour. Technol. 109, 261–5. doi:10.1016/j.biortech.2011.07.025

90. Sorokin, C., Krauss, R.W., 1958. The Effects of Light Intensity on the Growth Rates of Green Algae. Plant Physiol. 33 , 109–113. doi:10.1104/pp.33.2.109

91. Tredici, M., Zittelli, G., 1998. Efficiency of sunlight utilization: tubular versus flat photobioreactors. Biotechnol. Bioeng. 57, 187–97.

92. Ungerer, J., Tao, L., Davis, M., Ghirardi, M., Maness, P.-C., Yu, J., 2012. Sustained photosynthetic conversion of CO2 to ethylene in recombinant cyanobacterium Synechocystis 6803. Energy Environ. Sci. 5, 8998. doi:10.1039/c2ee22555g

93. Wang, C.-Y., Fu, C.-C., Liu, Y.-C., 2007. Effects of using light-emitting diodes on the cultivation of Spirulina platensis. Biochem. Eng. J. 37, 21–25. doi:10.1016/j.bej.2007.03.004

94. Wijffels, R.H., Barbosa, M.J., 2010. An outlook on microalgal biofuels. Science 329, 796–9. doi:10.1126/science.1189003

95. Wijffels, R.H., Barbosa, M.J., Eppink, M.H.M., 2010. Microalgae for the production of bulk chemicals and biofuels. Biofuels Bioprod. Biorefining 4, 287–295. doi:10.1002/bbb

96. Yun, Y.-S., Lee, S.B., Park, J.M., Lee, C.-I., Yang, J.-W., 1997. Carbon Dioxide Fixation by Algal Cultivation Using Wastewater Nutrients. J. Chem. Technol. Biotechnol. 69, 451–455. doi:10.1002/(SICI)1097-4660(199708)69:4<451::AID-JCTB733>3.0.CO;2-M

97. Yusuf, C., 2007. Biodiesel from microalgae. Biotechnol. Adv. 25, 294–306. doi:10.1016/j.biotechadv.2007.02.001

98. Zhao, Y., Wang, J., Zhang, H., Yan, C., Zhang, Y., 2013. Effects of various LED light wavelengths and intensities on microalgae-based simultaneous biogas upgrading and digestate nutrient reduction process. Bioresour. Technol. 136, 461–8. doi:10.1016/j.biortech.2013.03.051

99. Ahuja, P. and M. Tatsutani (2009) "Sustainable energy for developing countries." S.A.P.I.EN.S **2**.

100. Anker, J. N., W. P. Hall, et al. (2008). "Biosensing with plasmonic nanosensors." Nature Materials **7**(6): 442-453.

101. Arora, P., A. Sindhu, et al. (2011). "Biosensors as innovative tools for the detection of food borne pathogens." Biosensors and Bioelectronics **28**(1): 1-12.

102. Barrios, C. A. (2009). "Optical Slot-Waveguide Based Biochemical Sensors." Sensors **9**(6): 4751-4765.

103. Campbell, M. (2008). "Biodiesel: Algae as a Renewable Source for Liquid Fuel." Guelph Engineering Journal **1**: 2-7.

104. Chao, C. Y., W. Fung, et al. (2006). "Polymer microring resonators for biochemical sensing applications." IEEE Journal of Selected Topics in Quantum Electronics **12**(1): 134-142.

105. Chao, C. Y. and L. J. Guo (2002). "Polymer microring resonators fabricated by nanoimprint technique." Journal of Vacuum Science & Technology B **20**(6): 2862-2866.

106. Chen, Y.-F., X. Serey, et al. (2012). "Controlled Photonic Manipulation of Proteins and Other Nanomaterials." Nano Letters.

107. Chinowsky, T. M., J. G. Quinn, et al. (2003). "Performance of the Spreeta 2000 integrated surface plasmon resonance affinity sensor." Sensors and Actuators B: Chemical **91**(1–3): 266-274.

108. Choi, C. J. and B. T. Cunningham (2006). "Single-step fabrication and characterization of photonic crystal biosensors with polymer microfluidic channels." Lab on a Chip **6**(10).

109. Choi, C. J. and B. T. Cunningham (2007). "A 96-well microplate incorporating a replica molded microfluidic network integrated with photonic crystal biosensors for high throughput kinetic biomolecular interaction analysis." Lab on a Chip **7**(5): 550-556.

110. Choi, M., J. W. Choi, et al. (2013). "Light-guiding hydrogels for cell-based sensing and optogenetic synthesis in vivo." Nat Photon **7**(12): 987-994.

111. Ding, L., R. I. Blackwell, et al. (2008). "Femtosecond laser micromachining of waveguides in silicone-based hydrogel polymers." Applied Optics **47**(17): 3100-3108.

112. Erickson, D., S. Mandal, et al. (2008). "Nanobiosensors: optofluidic, electrical and mechanical approaches to biomolecular detection at the nanoscale." Microfluid. Nanofluid. **4**(1-2): 33-52.

113. Erickson, D., X. Serey, et al. (2011). "Nanomanipulation using near field photonics." Lab on a Chip **11**(6): 995-1009.

114. Erickson, D., D. Sinton, et al. (2011). "Optofluidics for energy applications." Nature Photonics **5**(10): 583-590.

115. Fan, C., Z. Q. Hu, et al. (2011). "Rapid detection of food- and waterborne bacteria using surface-enhanced Raman spectroscopy coupled with silver nanosubstrates." Applied Microbiology and Biotechnology **92**(5): 1053-1061.

116. Fan, X. D. and I. M. White (2011). "Optofluidic microsystems for chemical and biological analysis." Nature Photonics **5**(10): 591-597.

117. Fu, E., P. Kauffman, et al. (2010). "Chemical signal amplification in two-dimensional paper networks." Sensors and Actuators B: Chemical **149**(1): 325-328.

118. Gopalakrishnan, N., K. S. Sagar, et al. (2010). "UV patterned nanoporous solid-liquid core waveguides." Opt. Express **18**(12): 12903-12908.

119. Hoang, S., S. Guo, et al. (2011). "Visible Light Driven Photoelectrochemical Water Oxidation on Nitrogen-Modified TiO2 Nanowires." Nano Letters **12**(1): 26-32.

120. Jacobson, M. Z. and M. A. Delucchi (2011). "Providing all global energy with wind, water, and solar power, Part I: Technologies, energy resources, quantities and areas of infrastructure, and materials." Energy Policy **39**(3): 1154-1169.

121. Kammen, D. (2006) "Bioenergy in Developing Countries: Experiences and Prospects." 2020 Vision For Food, Agriculture, and the Environment.

122. Kuhn, S., B. S. Phillips, et al. (2010). "Ultralow power trapping and fluorescence detection of single particles on an optofluidic chip." Lab on a Chip **10**(2): 189-194.

123. Larkum, A. W. D., I. L. Ross, et al. (2012). "Selection, breeding and engineering of microalgae for bioenergy and biofuel production." Trends in Biotechnology **30**(4): 198-205.

124. Lee, J. S., S. H. Lee, et al. (2011). "Artificial photosynthesis on a chip: microfluidic cofactor regeneration and photoenzymatic synthesis under visible light." Lab on a Chip **11**(14).

125. Ling, T., S.-L. Chen, et al. (2011). "Fabrication and characterization of High Q polymer micro-ring resonator and its application as a sensitive ultrasonic detector." Optics Express **19**(2): 861-869.

126. Mancuso, M., J. M. Goddard, et al. (2012). "Nanoporous polymer ring resonators for biosensing." Optics Express **20**(1): 245-255.

127. Mandal, S., J. M. Goddard, et al. (2009). "A multiplexed optofluidic biomolecular sensor for low mass detection." Lab on a Chip **9**: 2924-2932.

128. Mathias, P. C., N. Ganesh, et al. (2008). "Application of Photonic Crystal Enhanced Fluorescence to a Cytokine Immunoassay." Analytical Chemistry **80**(23): 9013-9020.

129. Measor, P., B. S. Phillips, et al. (2011). "Tailorable integrated optofluidic filters for biomolecular detection." Lab on a Chip **11**(5): 899-904.

130. Nam, J.-M., C. S. Thaxton, et al. (2003). "Nanoparticle-Based Bio--Bar Codes for the Ultrasensitive Detection of Proteins." Science **301**(5641): 1884-1886.

131. Olsen, E. V., C. S. Gibbins, et al. (2009). "Real-Time FRET PCR Assay for Salmonella enterica Serotype Detection in Food." Military Medicine **174**(9): 983-990.

132. Ooms, M. D., V. J. Sieben, et al. (2012). "Evanescent photosynthesis: exciting cyanobacteria in a surface-confined light field." Physical Chemistry Chemical Physics **14**(14): 4817-4823.

133. Reece, S. Y., J. A. Hamel, et al. (2011). "Wireless Solar Water Splitting Using Silicon-Based Semiconductors and Earth-Abundant Catalysts." Science **334**(6056): 645-648.

134. Searchinger, T., R. Heimlich, et al. (2008). "Use of U.S. Croplands for Biofuels Increases Greenhouse Gases Through Emissions from Land-Use Change." Science **319**(5867): 1238-1240.

135. Smith, E. J., S. Schulze, et al. (2011). "Lab-in-a-Tube: Detection of Individual Mouse Cells for Analysis in Flexible Split-Wall Microtube Resonator Sensors." Nano Letters **11**(10): 4037-4042.

136. Smith, E. J., W. Xi, et al. (2012). "Lab-in-a-tube: ultracompact components for on-chip capture and detection of individual micro-/nanoorganisms." Lab on a Chip **12**: 1917-1931.

137. Storhoff, J. J., R. Elghanian, et al. (1998). "One-Pot Colorimetric Differentiation of Polynucleotides with Single Base Imperfections Using Gold Nanoparticle Probes." Journal of the American Chemical Society **120**(9): 1959-1964.

138. Storhoff, J. J., A. D. Lucas, et al. (2004). "Homogeneous detection of unamplified genomic DNA sequences based on colorimetric scatter of gold nanoparticle probes." Nat Biotech **22**(7): 883-887.

139. Tan, Y., C. Ge, et al. (2011). "Plastic-Based Distributed Feedback Laser Biosensors in Microplate Format." Sensors Journal, IEEE **PP**(99): 1-1.

140. Taton, T. A., C. A. Mirkin, et al. (2000). "Scanometric DNA Array Detection with Nanoparticle Probes." Science **289**(5485): 1757-1760.

141. Wilson, R. (2008). "The use of gold nanoparticles in diagnostics and detection." Chemical Society Reviews **37**(9): 2028-2045.

142. Yang, A. H. J. and D. Erickson (2010). "Optofluidic ring resonator switch for optical particle transport." Lab on a Chip **10**(6): 769-774.

143. Yang, A. H. J., S. D. Moore, et al. (2009). "Optical manipulation of nanoparticles and biomolecules in sub-wavelength slot waveguides." Nature **457**(7225): 71-75.

144. Yanik, A. A., A. E. Cetin, et al. (2011). "Seeing protein monolayers with naked eye through plasmonic Fano resonances." Proceedings of the National Academy of Sciences **108**: 11784-11789.